January 2020

On The Potential Of Lignin As A Sintering Aid And Binder For Designing Porous Foams

Grant Christian Ellis

ON THE POTENTIAL OF LIGNIN AS A SINTERING AID AND BINDER FOR DESIGNING POROUS FOAMS

by

Grant Christian Ellis
Bachelor of Science, University of North Dakota, 2018

A Thesis

Submitted to the Graduate Facility

of the

University of North Dakota

In partial fulfillment of the requirements

for the degree of

Master of Science
in
Mechanical Engineering

Grand Forks, North Dakota
August
2020

Name: Grant Ellis

Degree: Master of Science

This document, submitted in partial fulfillment of the requirements for the degree from the University of North Dakota, has been read by the Faculty Advisory Committee under whom the work has been done and is hereby approved.

DocuSigned by:
Surojit Gupta
Surojit Gupta

DocuSigned by:
Yun Ji
Yun Ji

DocuSigned by:
Clement Tang
Clement Tang

This document is being submitted by the appointed advisory committee as having met all the requirements of the School of Graduate Studies at the University of North Dakota and is hereby approved.

DocuSigned by:
Chris Nelson
Chris Nelson
Dean of the School of Graduate Studies

8/11/2020
Date

Title	On the Potential of Lignin as a Sintering Aid and Binder For Designing Porous Foams
Department	Mechanical Engineering
Degree	Master of Sciences

In presenting this thesis in partial fulfillment of the requirements for a graduate degree from the University of North Dakota, I agree that the library of this University shall make it freely available for inspection. I further agree that permission for extensive copying for scholarly purposes may be granted by the professor who supervised my thesis work or, in her/his absence, by the Chairperson of the department or the dean of the Graduate School. It is understood that any copying or publication or other use of this thesis or part thereof for financial gain shall not be allowed without my written permission. It is also understood that due recognition shall be given to me and to the University of North Dakota in any scholarly use which may be made of any material in my thesis.

Grant Ellis
8/11/2020

TABLE OF CONTENTS

LIST OF FIGURES

Figure Page

LIST OF TABLES

ACKNOWLEDGEMENTS

Firstly, I would like to thank my friends and family for their unending support during the long and challenging journey in my pursuit of Master of Science in Mechanical Engineering. I owe this success to their love and encouragement, which has enabled me to overcome great adversity.

I am very honored and privileged to have been a part of the Material Science Research Team, under Dr. Surojit Gupta and the Department of Mechanical Engineering at the College of Engineering and Mines. Thank you, Dr. Gupta, for your constant dedication to my research and education. As a student at the University of North Dakota, you have been my greatest advocate! Thank you for accepting me into the Graduate Program and for all your guidance, patience, and teachings throughout my collegiate career.

To my committee members, Dr. Clement Tang and Dr. Yun Ji, I would like to thank you for your participation and consultation with my graduate research. It means an incredible amount to me that you would accept my invitation to become members and allow my pursuit of a Graduate Degree.

I would like to thank the Mechanical Engineering Department, Dean Professorship, and North Dakota Corn Council for funding my research. Your contribution to the Material Science Laboratory is not only appreciated, but also recognized as a vital constituent of this establishment and its activities.

Special thank you to Brian and Shelley Worley,
Who made my degree path possible!

ABSTRACT

Lignin, as an abundant source of bio-renewable material, has been a subject of investigation for many years. Due to its chemically heterogenous and recalcitrant nature, 98% of the material is discarded as waste [3]. Laboratory groups have been exploring lignin's potential as a value-added ingredient to promote biocompatibility, biodegradation, and substitute toxic, petroleum-based materials [4,6]. In our laboratory, lignin has been utilized as precursor for carbon foam, yielding highly porous structures after pyrolysis [5], and has also been shown to be compatible with other bio-waste materials [8]. The next stage of research focusses on controlled additions of Cu or Distiller's Dried Grains with Solubles (DDGS) to reinforce lignin during pyrolysis. To achieve the goal of enhancing and controlling the properties of pyrolyzed lignin, Cu was used as a base metal for designing scaffolds. As an associated bio-waste material, DDGS has been shown to have significant commercial potential beyond edible materials [14-20]. Separate additions of these materials are combined with lignin using similar design principles for manufacturing, methodology of fabrication, and characterization. In both composite systems, lignin is observed to be a low temperature sintering aid, or pore former, while acting as a strong mechanical binder. Cu or DDGS additions within a lignin matrix resulted in strength enhancement as compared to fabricated lignin foams while achieving highly porous composite foams. Such foams exhibit temperature-controlled wettability, resulting in hydrophobic behavior when fabricated at 300 °C, or hydrophilic behavior when fabricated at 900 °C. The research concludes that Cu and DDGS can be effective reinforcements into lignin-based carbon foams. In addition, lignin can be a low-temperature sintering aid which is derived from bio-renewable sources.

CHAPTER 1: INTRODUCTION AND BACKGROUND

The re-utilization of lignin has been a subject of investigation within the field of Material Science for many years. Lignin is a biopolymer made up of three phenylpropane monomers: 1) coumaryl, 2) coniferyl, and 3) sinapyl alcohols. The lignin molecule contains zero, one, and two methoxyl groups, respectively, in addition to all the monomers containing hydroxyl groups [1]. It is this structure that forms a recalcitrant polymer with high molecular weight and chemical heterogeneity. Commercially, lignin is a biproduct of the Kraft Pulping process [2], however due to its chemically heterogenous and recalcitrant nature, 98% of the material is discarded as waste [3]. Therefore, novel methods are required for its re-utilization. Along with cellulose and hemicellulose, lignin is a predominant constituent of biomass that can be found in all vascular plants [2]. Thus, lignin is a vastly abundant biomaterial; as such, it offers great potential as a renewable source for the design of novel materials. Many groups have been investigating means of utilizing lignin for value-added applications.

1.1 Lignin Utilization Within Foams

In a 2016 publication, Mahmood et al. [4] explored the infiltration of lignin into polyurethane (PU) foams. The objective was to prepare polyols and rigid polyurethane (RPU) foams from lignin [4]. Initial studies showed that the addition of more than 20-30 wt. % lignin caused deterioration in strength of RPU foams. Lignin depolymerization allowed 50% replacement. This modification allowed lignin to replace 50 wt. % of the petroleum polyols, while improving the physical and thermal stability of the foam as compared to commercial Rigid PU (RPU) foams. Oxypropylation method allowed for the preparation of Bio-RPU foams with replacement ratios up to 70 wt. %.

The resulting foam showed low density, promising strength, and low thermal conductivity which showed promised a potential insulation material. Despite the enhancements in bio-replacement and the mechanical properties depolymerized lignin has on PU foams, Mahmood et al. [4] recommend that further research is needed to improve the morphological characteristics with increased bio replacements. This is a similar issue found with the pyrolysis of lignin [5]. The authors also mention that the costly processes of depolymerizing the lignin, which requires high temperatures and pressures, makes it impractical for scaling up this application to an industrial level [4].

Lignin has also been used within hydrogels, as reviewed by Meng et al. [6], to increase the biocompatibility and biodegradability of the material, along with valorizing lignin and its derivatives. Lignin-based hydrogels can be stabilized by cross-linking by copolymerization, or crosslinking between reactive polymer precursors, or crosslinking via polymer-polymer reaction. Commonly explored applications of these materials are as absorbents for heavy metal ions, and as agents for controlled water retention and delivery. While the synthesis and characterization of lignin-based hydrogels is well understood, Meng et al. [6] identify several obstacles for the commercial utilization of these materials, namely, (a) simplification and cost reduction of the manufacturing process, and (b) heterogeneity of lignin which affect the stability and integrity of these hydrogels [6].

1.2 Lignin Based Carbon Foams

In a recent publication, Gupta et al. [5] characterized a new means of fabricating carbon foam by the pyrolysis of as received Indulin lignin. The experimentation featured loosely packed lignin samples that were pyrolyzed at four separate temperatures for one hour. The temperatures ranged at 300°, 500°, 700°, and 900° C. The result of this procedure yielded a highly porous

structure that is detailed by the images in Fig. 1.1 [5]. *Please note, the presence of huge macropores at the center of these samples.*

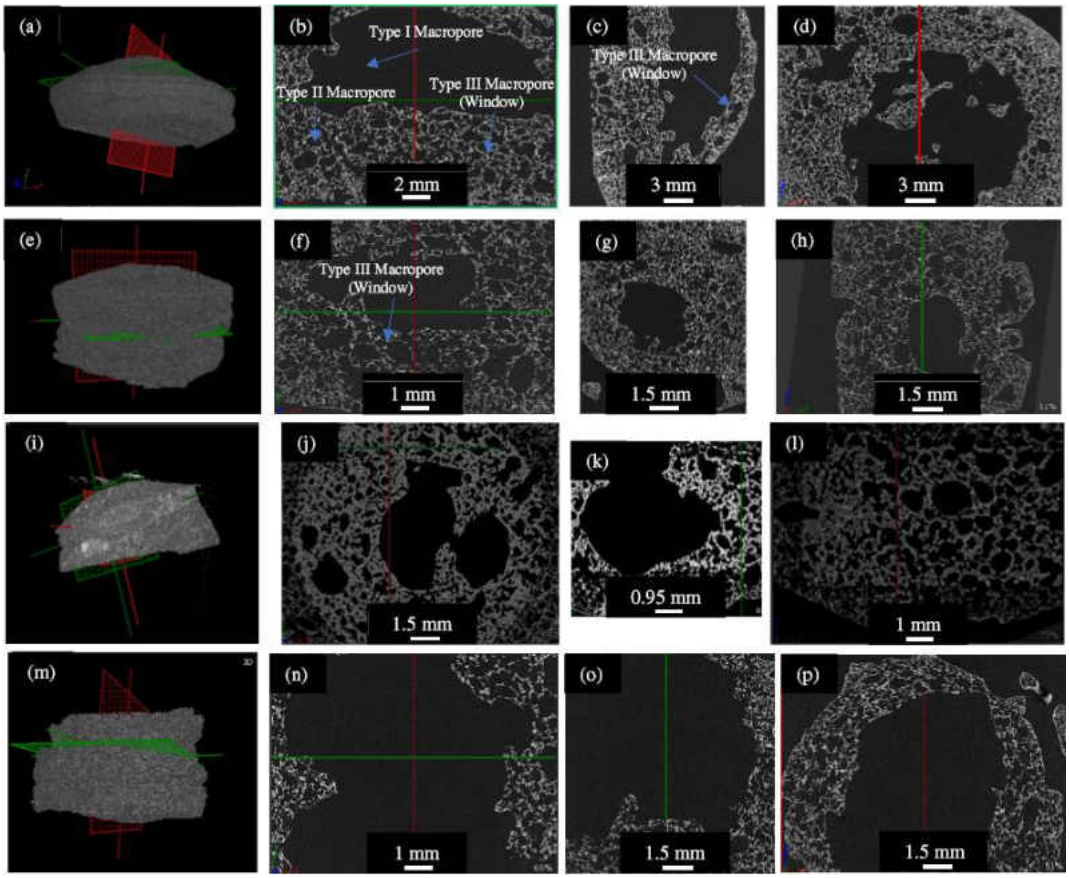

Figure1.1: X-ray tomography of samples pyrolyzed at: 300°C, showing (a) 3D view, and (b)-(d) cross-sections; 500°C, showing (e) 3D view, and (f)-(h) cross-sections; 700°C, showing (i) 3D view, and (j)-(l) cross-sections; and 900°C, showing (m) 3D view, and (n)-(p) cross-sections (*this image is used for criticism under fair usage*).

The key observation is lignin being very effective at forming an expanded foam when subjected to pyrolysis. This is the case regardless to the pyrolysis temperature, as all the samples ranging from 300°C to 900°C feature a total porosity greater than 90% [5]. This is due to lignin having a broad temperature range for decomposition, as seen in Fig 1.2 [7].

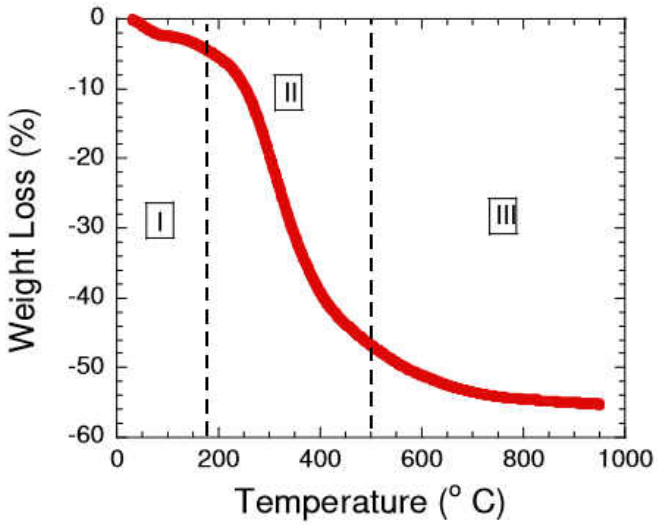

Figure 1.2: Thermogravimetric analysis (TGA) of Indulin lignin (*this image is used for criticism under fair usage*).

Figure 1.2 displays the results of thermogravimetric analysis (TGA) of Indulin lignin, ranging from 25°C to 900°C [7]. Here, three stages of decomposition have been defined. Stage I occurs at 25°C-170°C, where absorbed water is dehydrated from the material. Stage II marks the beginning of pyrolysis at 160°C. At this point, internal links experience decomposition and gasses (such as water, carbon dioxide, and methane) are released [5]. This continues until 500°C, where lignin undergoes complete pyrolytic degradation during stage III.

The expansion of lignin during pyrolysis across a large temperature range, and as low as 300°C, is a key feature in the re-utilization of lignin as a precursor for carbon foam. It grants the fabrication of carbon foam at low temperatures, along with controlling the nature of the expansion

by only adjusting the fabrication temperature. Consistency between TGA and FTIR analyses of pyrolyzed lignin supports this claim by detailing unique changes at each temperature.

In the same study, Gupta et al. [5] explored the mechanical behaviors of the lignin carbon foams. It has been demonstrated that the adjustment of the pyrolysis temperature changes the chemical nature of the material. Further investigation shows that this adjustment influences the mechanical behavior of the foams. Particularly, the structure and wettability of the foams experience transition as the pyrolysis temperature increases. This occurs while overall maintaining the porosity and strength of the material.

Using scanning electron microscopy (SEM) imaging, it is observed that the pyrolyzed lignin yields an ideal structure for a carbon foam [5]. In this study, it was also observed that the material experiences a transition from hydrophobic when fabricated at 300°C and 500°C, to hydrophilic when fabricated at 700°C and 900°C.

As mentioned, the transitions of the cellular structure and wettability do not come at the sacrifice of the strength, nor porosity of the foams. Figure 1.3 [5] plots the average ultimate compressive strength (UCS) of the foams fabricated at 300°C through 900°C. For each fabrication temperature, the UCS is maintained at more than 0.5 MPa with strength recovery at just under 1 MPa for fabrication temperatures at above 700°C.

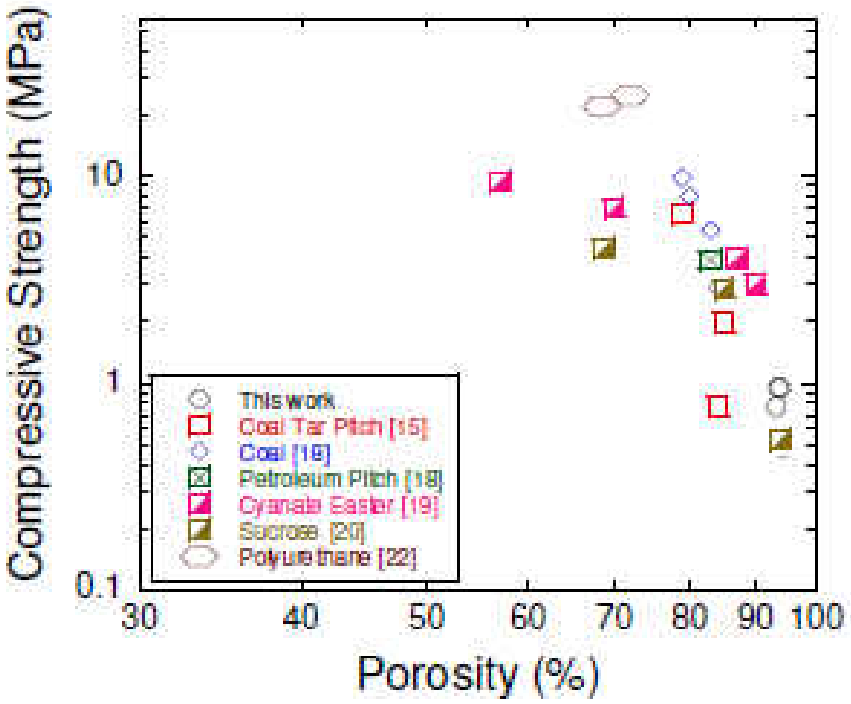

Figure 1.3: Plot of compressive strength versus porosity of different foams [5] (*this image is used for criticism under fair usage*; please refer to the paper for cited references).

This demonstrates that lignin carbon foam has tremendous potential for re-utilization, which may compete with conventional materials.

With the goal of controlling the expansion of lignin during pyrolysis and enhancing the mechanical properties of the resulting carbon foam, Gupta et al. [8] reinforced the foam with sugar beet pulp (SBP) and wheat straw (WS). These materials are abundant agricultural waste products, maintaining the biocompatibility of a lignin-based carbon foam. Lignin powder is combined with 50 wt. % SBP or WS powders and are then mixed with 10 wt. % deionized water as a binder. The mixtures are cold pressed to form a green body and are then placed in an argon furnace for pyrolysis. As with the fabrication of pure lignin-based foam, these composites are fabricated at 300, 500, 700, and 900 °C. Similar to pure lignin-based carbon foams, FTIR analysis of the two composite systems show that the foams are aromatic in nature [8]. Compression testing was

repeated for these composite systems to investigate the effects the agricultural additives had on the mechanical performance on lignin-based carbon foam. The results for the average ultimate compressive strength (UTS) is detailed in Table 1.1 [8].

Table 1.1: UCS of SBP-Lignin and WS-Lignin Composite Systems (*this table is used for criticism under fair usage*) [8]

Ultimate Compressive Strength (MPa)				
Pyrolysis Temp. (°C)	300	500	700	900
SBP	1.31 ± 0.59	1.03 ± 0.52	1.14 ± 0.35	2.03 ± 1.23
WS	20.4 ± 13	13.1 ± 3.86	14.9 ± 7.26	27.6 ± 10.08

Strength enhancement is strongly gained with the addition of WS into the pyrolyzed lignin matrix. However, in the case of SBP addition the reinforcement fails to enhance the mechanical properties, maintaining the ultimate compressive strength at 1-2 MPa [8]. Overall, the strength enhancement is temperature dependent, with SBP not strengthening the matrix until fabrication at 900 °C and WS addition experiencing strength reduction between fabrication at 500 °C and 700 °C.

These experiments achieved the formation of lignin-based carbon foams while infiltrated with agricultural waste products. Like the pure lignin foams, these composites displayed temperature-dependent wettability, preserving the lignin's unique ability of property tailoring by adjustment of the pyrolysis temperature [8]. The most desired being the fabrication of a highly porous foam, with increased compressive strength and a uniform cellular structure. WS addition does yield promising results with its strength enhancement and uniform morphology. This prompts further exploration into the addition of agricultural waste products into lignin-based carbon foam. Though, from the results of these experiments, it is desired to continue the search for alternative additive materials. A new strategy is envisioned using copper particulates as reinforcement, while

DDGS addition, an agricultural waste product, is investigated in parallel. These two additive materials are what define the next phase of research into lignin-based carbon foams.

1.3 Construction of the Thesis

Chapter 2 explores copper-lignin composite systems, fabricated through pyrolysis of combined powders. The volume fraction and pyrolysis temperature of the lignin is adjusted to explore its interaction with copper. The composites are then characterized through mechanical testing. Experiments include porosity measurements, compression testing, wettability experiments, and hardness testing. The degradation of lignin is also explored with FTIR and TGA experiments. Chapter 3 explores Distiller's dried grains with solubles (DDGS)-lignin composites using similar design principles for manufacturing, methodology of fabrication, and characterization.

1.4 On the Selection of Copper

In order to achieve the goal of enhancing and controlling the properties of pyrolyzed lignin, it was determined that a metal would have the proper mechanical interaction due to its high molecular weight and the nature of metallic bonds. Candidate metals were primarily selected by a few criteria to avoid limiting the application of the composites. The metal was needed to be non-toxic, abundant, readily available, and of low cost. These traits would only promote the utilization of the composites. Keeping in mind the vision of fabricating carbon-based foams, the metal must not be able to form a carbon alloy. This also makes the project quite novel by combining metal and carbon in an otherwise imposable way. Next, the most obvious potential application of these composites is liquid filtration, so the metal should have anti-microbial properties in order to enhance this functionality. Finally, in a preliminary round of testing, Cu-lignin composites showed promising features where these composites showed no surface cracking and maintained its

cylindrical shape. By satisfying the described criteria, Cu was selected to be the ingredient for lignin composites.

1.5 On the Addition of DDGS

In a parallel study, investigation into the reutilization of byproducts from biomass is expanded to include distiller's dried grains with solubles (DDGS). The material is specifically the waste product of the extraction of ethanol from corn. While DDGS can include waste material from other plant sources, here it is used to specifically describe that of corn. In preliminary testing, DDGS is subjected to pyrolysis with the same conditions used for the pyrolysis of lignin in section 1.2. However, the green body and the pyrolyzed material of DDGS is delicate – often exhibiting signs of ware, flaking, and cracking. The material needs a binder agent to form mechanically stable pyrolyzed samples. When lignin is added to the material, it is found to result in a robust carbon foam. Such phenomenon prompted the exploration into lignin-DDGS systems.

CHAPTER 2: SYNTHESIS AND CHARACTERIZATION OF NOVEL Cu-LIGNIN COMPOSITES

2.1 Introduction

In this chapter, we will focus on designing Cu-Lignin composites. The goal of this chapter is to, (a) fabricate and characterize copper-lignin composite systems, and (b) characterize the material properties including porosity, strength, and wettability. Figure 2.1 shows the schematics of microstructure designed during this study.

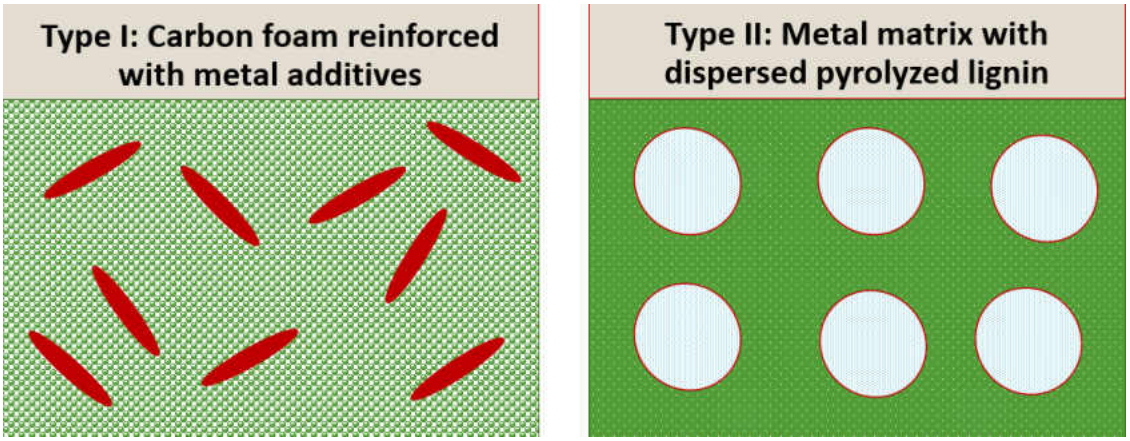

Figure 2.1: Schematic of Types I and II Composites.

In type-I composites, lignin derived carbon foam matrix will be reinforced with Cu additives. In type-II composites, Cu-matrix will be dispersed with pyrolyzed lignin. The hypothesis is thus two-fold:

- In type-I, Cu additions reinforce the lignin matrix and control the thermal expansion of lignin during pyrolysis;
- Due to above mentioned reasons, we will have better properties in type-I composites as compared to pyrolyzed lignin biofoams;

- In type-II composites, the addition of lignin will act as a poreformer with carbonaceous network for the formation of porous metals.

In conjunction to the independent hypotheses above, it is hypothesized that there will be no chemical interaction between the lignin and copper during any stage of the fabrication process – that the characteristics of pure pyrolyzed lignin previously identified will remain constant.

2.2 Experimental Details

2.2.1 Material Fabrication

Powders of Copper (Lot G12Z031, -325 mesh, 99% (metal basis), Alfa Aesar, Havehill, MA) and lignin (Indulin AT, MeadWestvaco, Richmond, VA) were ball milled (8000 M mixer Mill, SPEX SamplePrep, Metuchen, NJ) for 5 min. The following volume fractions were used during this study: (a) Type-I Composites; 10% copper to 90% lignin (Cu(10)-L(90)) and 25% copper to 75% lignin (Cu (25)-L75)), and (b) Type-II Composites; 50% copper to 50% lignin (Cu(50)-L (50)) and 75% copper to 25% lignin (Cu(75)-L(25)).

Each composition containing a set of samples were pyrolyzed at four separate temperatures; 300 °C, 500 °C, 700 °C, and 900 °C. The samples will be referred to as the following code: Cu(10)-L(90) (300 ^{o}C). The mixed powders were then filled in a 12.7 mm die. The pressed samples were then cold pressed (Model 3853-0, Carver Inc., Wabash, IN) at ~263 MPa for 30 s (this cycle was repeated twice). The samples were then pyrolyzed in a tube furnace at the designated temperature for 1h. To further decrease the probability of oxidization, Ti powder were placed at each end of the furnace, adjacent to the seals. All the experiments were performed at heating rate of 10 °C/min. The sample was removed from the furnace once the furnace temperature reaches below 100 °C. Finally, the top surface of each sample was polished until 1200 grit

finishing for Type I Composites and until ~1 μm finishing for Type II. This procedure is also used to make pure copper samples, using unmixed copper powder, to fabricate control specimens. Please refer to ref. [8] for details about the characterization procedure.

2.2.2 Microscopy Analysis

The microstructures of the composites were observed by Scanning Electron Microscope (SEM, JEOL JSM- 168 6490LV, JEOL USA, Inc., Peabody, Massachusetts) in secondary electron (SE) and backscattered electron (BSE) mode. Au/Pd (sputter coater, BAL-TEC RMC, Tucson, AZ) coated samples were used for chemical analysis. The chemical information is reported in Table 2.1. Like reported in ref. [8], the chemical readings of point of interest (PoI) was obtained by using a thermo nanotrace energy-dispersive X-ray detector with NSS-300e acquisition in a point analysis mode. For every PoI, an average of three readings is reported in the text.

2.2.3 Helium Pycnometry

True density (ρ_t) was obtained by performing Helium Pycnometry (Ultrapyc 1200e, Quantochrome Instruments, Boynton Beach, Florida) of the crushed powders.

2.2.4 Porosity Analysis

Initially, the top surfaces of the pyrolyzed cylindrical samples were machined to ensure an even surface, if needed. The dimensions (height (h) and diameter (d)), are measured by using a digital caliper. Each measurement is performed in three random locations. The mass of the sample is measured using a digital scale and recorded. The volume of the sample is then estimated using:

$$V = \frac{\pi D^2 h}{4} \text{ ----------(Eq. 2.1)}$$

where D is the average diameter and h is the average height. The average bulk density is calculated using:

$$\rho = \frac{m}{V} \text{ ----------(Eq. 2.2)}$$

where m is the mass and V is the calculated volume.

The porosity of the sample was calculated by using:

$$P = \left(1 - \frac{\rho}{\rho_t}\right) \times 100\% \text{ ----------(Eq. 2.3)}$$

Where ρ_t is the true density as measured by Helium Pycnometry. Please refer to Ref. 8 for the detailed procedure.

2.2.5 Fourier-Transform Infrared Spectroscopy (FTIR)

The specimens are manually ground into powder after the initial fabrication process. FTIR (Thermo Scientific Nicolet 8700 instrument) analysis on powders was performed on pyrolyzed powders by using the procedure described in Ref. [8].

2.2.6 Thermomechanical Analysis (TMA)

TMA (TMA 60 H, Shimadzu Scientific Instruments, Columbia, MD) analysis was performed on green compacts by using the procedure described in ref. [8].

2.2.7 Compression Testing

For compression testing, samples were machined into 5 x 5 x 5 mm^3 cubes. The samples were then tested by using a mechanical testing system (Shimadzu AD-IS UTM, Shimadzu Scientific Instruments Inc., Columbia, MD) at a deflection rate of 1 mm/min. The compressive

force and the deflection of the crosshead was measured by the machine. The resulting stress was calculated by using

$$\sigma = \frac{F}{A} \text{----------(Eq. 2.4)}$$

where F was the measured force and A was the average cross-sectional area of the specimen. The dimensions of the cubes were measured by using digital calipers, and include the length, width and height. The length and width were measured in three random locations. Thus, the average cross-sectional area is estimated to be

$$A = W \times L \text{----------(Eq. 2.5)}$$

where W and L are the average width and length, respectively. This procedure is repeated with three to five specimens from each of the composite systems. In addition, this procedure is performed on pure copper specimens as a control. Data from three sets of three copper specimens fabricated at 500 °C, 700 °C, and 900 °C is reported. See Table A1.1 for the trial counts at each condition. Copper samples fabricated at 300 °C were too brittle to be machined. Due to this reason, compression testing of the samples could not be performed.

Figure 2.2: Fractured copper samples fabricated at 300 °C.

2.2.8 Hardness Testing

Vicker's micro-hardness indenter (Mitutoyo HM-112, Mitutoyo Corporation, Aurora, IL) was used to test hardness by applying a load of 0.5 Kg for 15s. Only Type-II composites samples and Cu were tested as Type-I composites were highly porous and indents could not be observed in the matrix. For each sample, an average of five data points were taken.

2.2.9 Wettability

Type-I Composites were machined by using 1200 grit sandpaper, and Type-II Composites were polished with 1 μm diamond solution. For determining the contact angle, the Sessile Drop Test by using a contact angle system (Data physics contact angle system, OCA 15Plus, Future Digital Scientific Corp, New York) was used. Please refer to ref. [8] about details of the procedure.

2.3 Results and Discussion

2.3.1 FTIR

Figure 2.3 shows the FTIR analysis of different lignin-Cu compositions. In general, the intensity decreases after treatment at different temperatures which indicates that lignin is decomposing at higher temperatures. Table 2.1 shows the peak IDs of Cu(10)-Lignin(90) composition treated at different temperatures. Please refer to ref. [8] regarding the peak identification of these peaks. Based on peak IDs, we did not observe any additional peak due to interaction with Cu. In addition, the compositions became aromatic at higher temperatures [8]. Currently, we are working on developing a FTIR map of biomass-based composites. The results will be published in follow up publication.

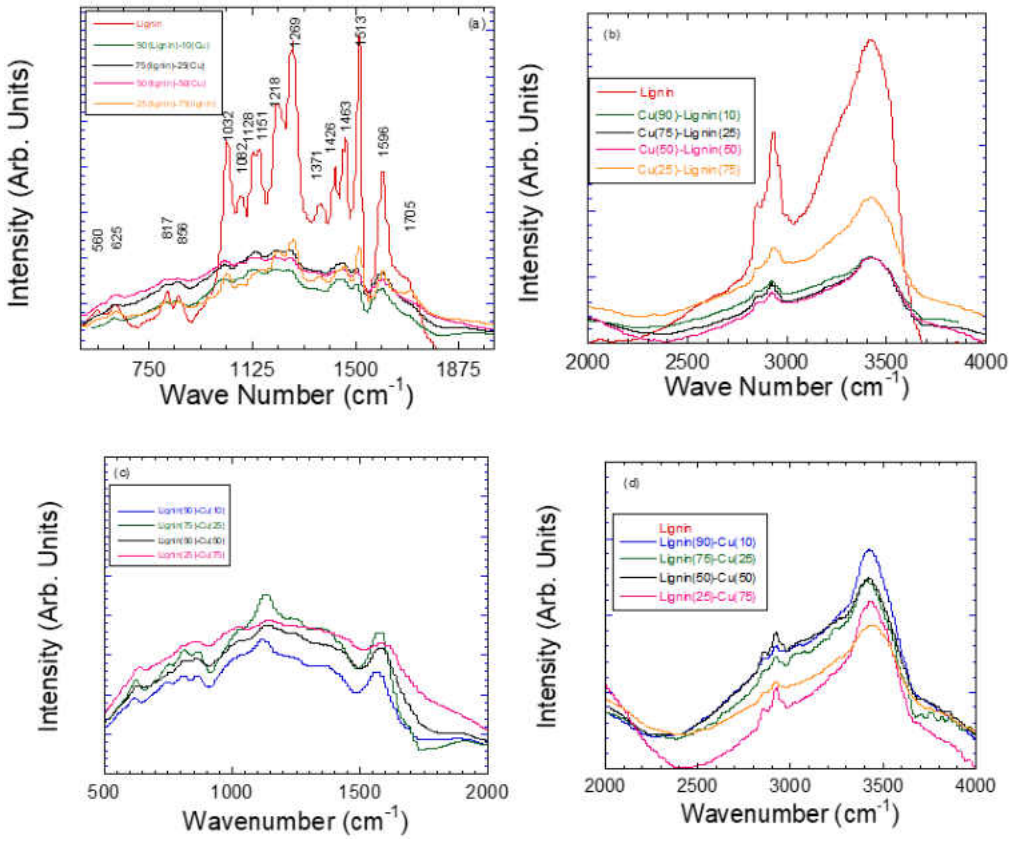

Figure 2.3: FTIR of Cu-L at, (a) 300 ºC (500-2000 cm^{-1}), (b) 300 ºC (2000-400 cm^{-1}), (c) 500 ºC (500-2000 cm^{-1}), (d) 500 ºC (2000-400 cm^{-1}), (e) 700 ºC (500-2000 cm^{-1}), (f) 700 ºC (2000-400 cm^{-1}), (g) 900 ºC (500-2000 cm^{-1}), and (h) 900 ºC (2000-400 cm^{-1}).

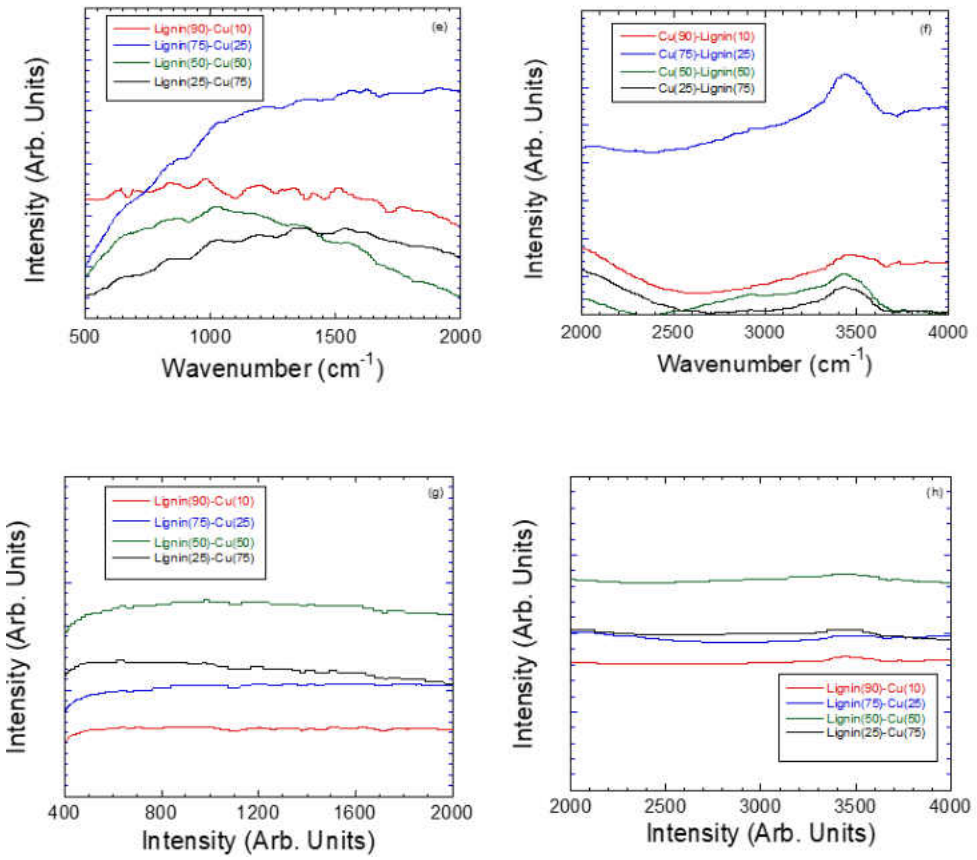

Figure 2.3: FTIR of Cu-L at, (a) 300 ºC (500-2000 cm^{-1}), (b) 300 ºC (2000-400 cm^{-1}), (c) 500 ºC (500-2000 cm^{-1}), (d) 500 ºC (2000-400 cm^{-1}), (e) 700 ºC (500-2000 cm^{-1}), (f) 700 ºC (2000-400 cm^{-1}), (g) 900 ºC (500-2000 cm^{-1}), and (h) 900 ºC (2000-400 cm^{-1}).

Table 2.1: FTIR peak IDs of lignin(90)-Cu(10) treated at different temperatures

Lignin	Lignin(90)-Cu(10) (300 °C)	Lignin(90)-Cu(10) (500 °C)	Lignin(90)-Cu(10) (700 °C)	Lignin(90)-Cu(10) (900 °C)
3424	3423	3429	3450, 3875, 3832, 3768, 3727	3832, 3727, 3437
3000	x			x
2934	2923	2923	x	2937
2850	2843	2848		
1707			1763	1769
1596	1593	1565	x	1629
1513	1502	x	1506	
1463	1451	x	x	x
1426	x	x	1407	1408
1371		1357		1335
1269	1257		x	
1218	1206	x	1198	1205
1151	1132		x	
1128		1117		x
1082	x	x	979	
			x	
1032	1021	1030		993
856	853	864	839	x
817	802	808, 747	x	
625	623	619	691, 645	646
560	x		507	x

2.3.2 Microstructure

SEM micrographs of each composite system are compiled in Figures 2.4-2.7. It can be observed that each composition yields similar microstructures to their counterparts across different pyrolysis temperatures. For example, Type-I composites Lignin(90)-Cu(10) composition fabricated at 300 °C (Fig. 2.3 (d)) showed cellular matrix reinforced with Cu particulates. No sign of reaction between Cu and lignin matrix was observed. Similar microstructure was obtained after pyrolysis at 500, 700, and 900 °C (Figs. 2.4-2.6), respectively.

In Type-II composites, we observed a structure that is counter to the hypothesis. Rather than expanding into a porous structure, the pyrolyzed lignin infiltrated into the intergranular space of the Cu-matrix and bonded the structure. This is a novel example of lignin where it can be used for binding Cu during pyrolysis. This phenomenon, and its consequences, are further explored in the following sections.

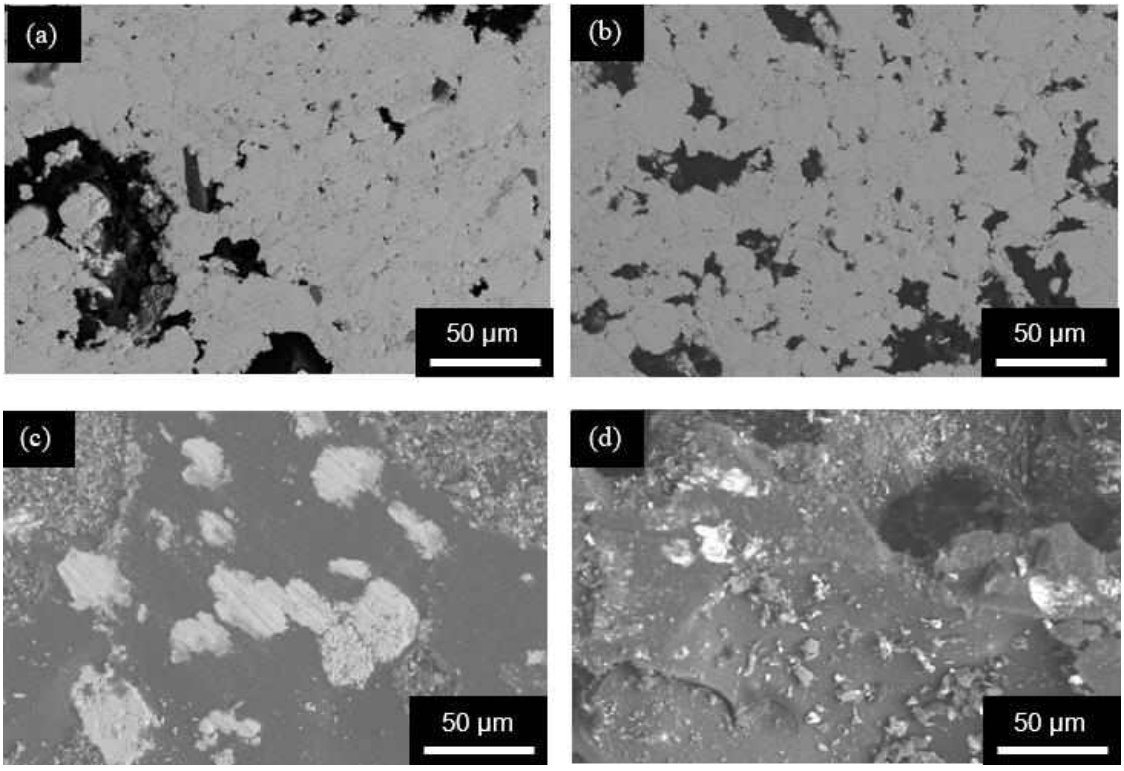

Figure 2.4: BSE SEM micrographs of, (a) Cu(75)-Lignin(25) , (b) Cu (50)-Lignin(50), (c) Cu (25)-Lignin(75), (d) Cu (10)-Lignin(90) of samples pyrolyzed at 300 ^{o}C.

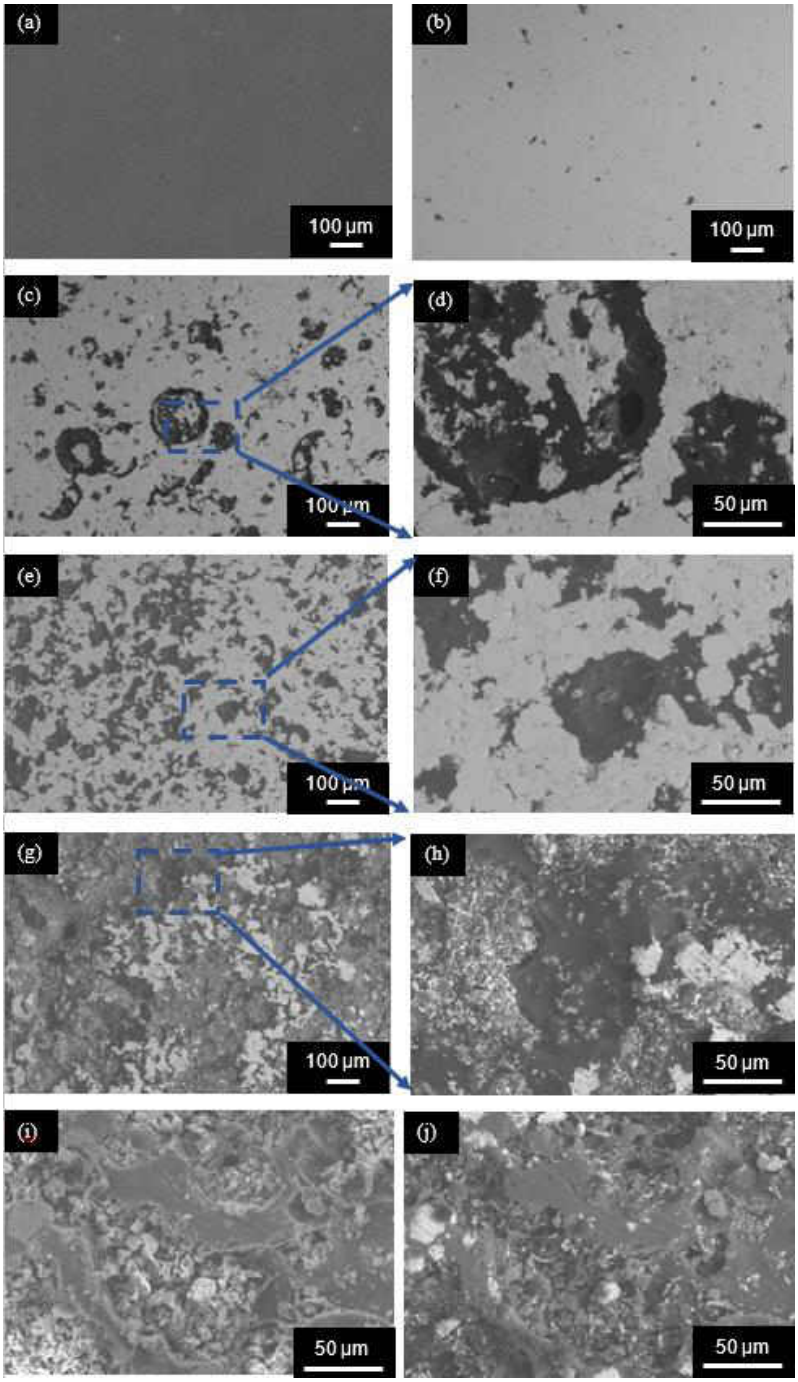

Figure 2.5: SEM micrographs of, (a) Cu in SE, (b) BSE image of the same region, (c) Cu (75)-Lignin(25) , (d) BSE image of (Cu (75)-Lignin(25) (higher magnification), (e) Cu (50)-Lignin(50), (f) Cu (50)-Lignin(50) (higher magnification), (g) BSE image of Cu (25)-Lignin(75), (h) Cu (25)-Lignin(75) (higher magnification), and (i) Cu (10)-Lignin(90) in SE, and (j) Cu (10)-Lignin(90) (BSE) of samples pyrolyzed at 500 ^{o}C.

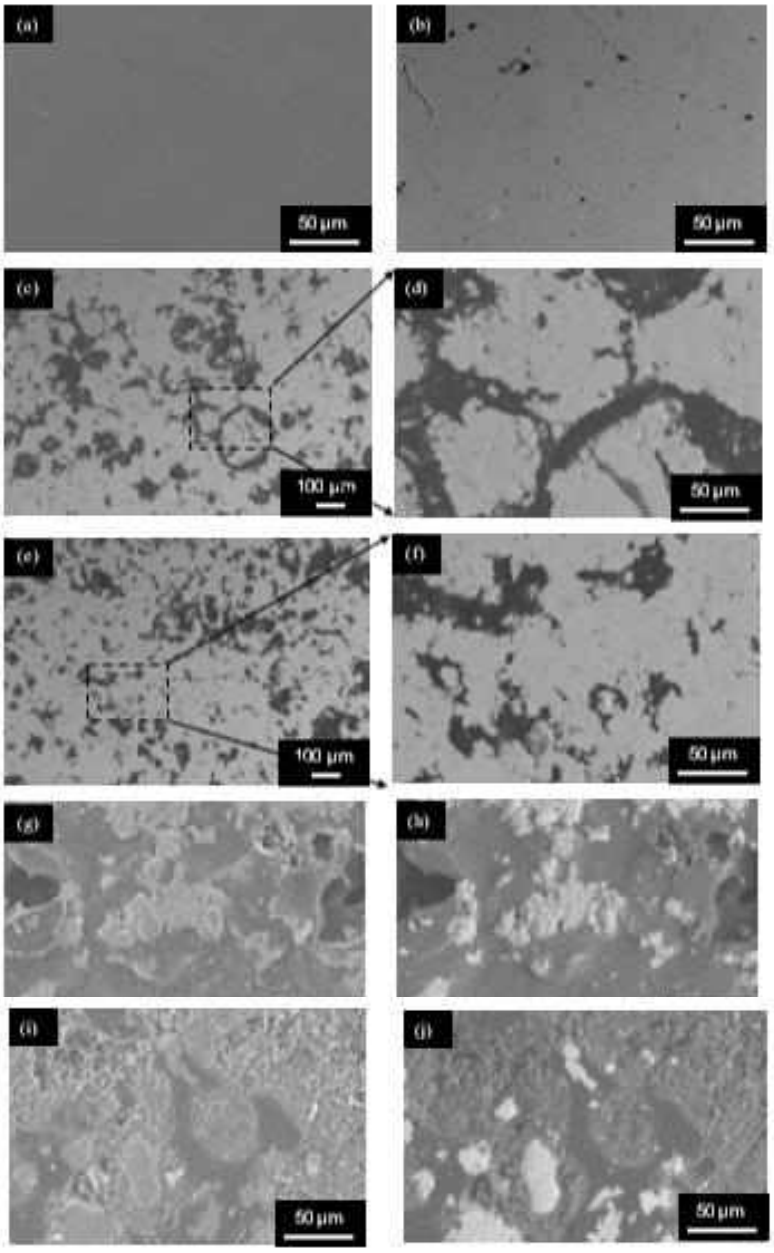

Figure 2.6: SEM micrographs of, (a) Cu in SE, (b) BSE image of the same region, (c) BSE image of Cu (75)-Lignin(25) , (d) (Cu (75)-Lignin(25) (higher magnification), (e) BSE image of Cu (50)-Lignin(50), (f) Cu (50)-Lignin(50) (higher magnification), (g) SE image of Cu (25)-Lignin(75), (h) Cu (25)-Lignin(75) (BSE) of samples pyrolyzed at 700 ^{o}C, (i) SE image of Cu (10)-Lignin(90), and (j) Cu (10)-Lignin(90) (BSE) of samples pyrolyzed at 700 ^{o}C.

.

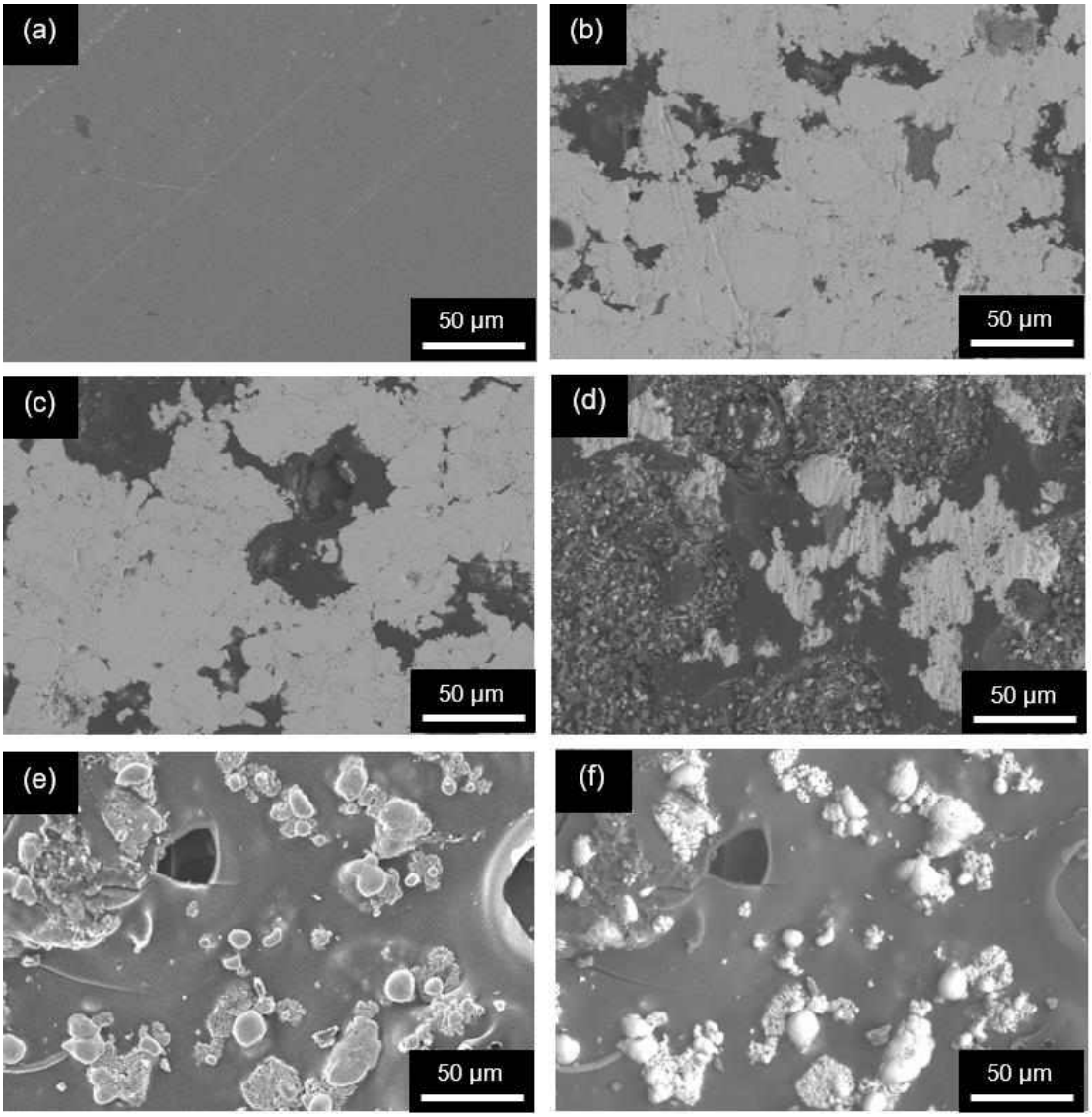

Figure 2.7: SEM micrographs of, (a) Cu in SE, (b) (Cu (75)-Lignin(25) in BSE , (c) Cu (50)-Lignin(50) in BSE, (d) Cu (25)-Lignin(75) in BSE, (e) Cu (10)-Lignin(90) (SE), and (f) Cu (10)-Lignin(90) (BSE) of samples pyrolyzed at 900 ^{o}C.

2.3.3 Porosity

Figure 2.8 shows the plot of porosity (%) versus lignin (%) concentration in Cu matrix as a function of different temperatures. Type-I composite, Lignin(90)-Cu(10), had porosity of ~83.2%, ~84.2%, ~85.3%, ~85.6 after pyrolysis at 300, 500, 700, and 900 ^{o}C, respectively. Similarly, Lignin(75)-Cu(25) compositions had porosity of ~67.2, ~67.1, ~69.6, and ~68.4%,

respectively after pyrolysis at 300, 500, 700, and 900 °C, respectively. Comparatively, pure lignin pyrolyzed at different temperatures have porosity in the range of 93-95% [5]. The reduction of porosity as the volume fraction of Cu is increased is due the presence of Cu which constrains the expansion of lignin matrix during pyrolysis. Another key observation is that the porosity of the Type-I composites is not a function of fabrication temperature. Because pure pyrolyzed lignin is observed to have temperature-dependent wettability behavior, it is important to note that the porosity of these composites will not be sacrificed during any such tailoring.

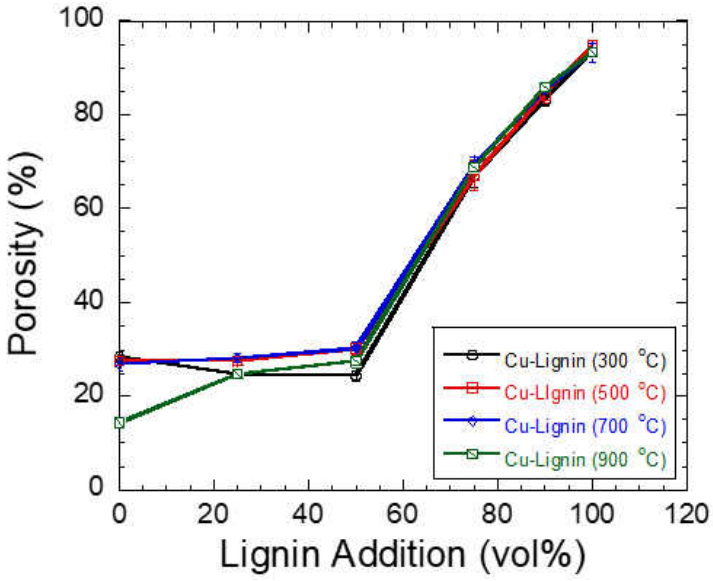

Figure 2.8: Plot of porosity (%) versus lignin additions (vol%).

The results of Type-II composites are in stark contrast to the former. As suggested by the micrographs, lignin is filling the voids within the copper matrix. For fabrication at 300 °C, lignin acts as a densification agent, decreasing the porosity of the copper matrix to ~24.4% with 50 vol. % addition of lignin. In the case of samples fabricated at 500 °C and 700 °C, this allowed for the porosity to be maintained at ~30.1 and ~30.4%, respectively in Cu(50)-Lignin(50) composites. Comparatively, Cu had porosity of 28.6%, 27.4% and 26.9% after sintering at 300, 500, and 700

^{o}C, respectively. Due to sintering and densification, Cu have ~14.5% porosity after treatment at 900 ^{o}C. However, despite the Cu matrix becoming sintered, the addition of lignin results in porosity of ~27.5% for the Cu(50)-Lignin(50) composite systems. Comparatively, Cu(75)-Lignin(25) had porosity of ~28.6, 27.4, ~26.9, and 14.5% after pyrolysis at 300, 500, 700, and 900 ^{o}C.

2.3.4 TMA

Figure 2.9 shows the TMA behavior of lignin [5]. Comparatively, Fig. 2.10 shows the TMA behavior of Cu-Lignin composites. Lignin deforms significantly between 200 and 300 °C which coincides with the pyrolytic-melting and solidification of lignin [[5]; please refer to this citation for detailed description of the process with corresponding citations].

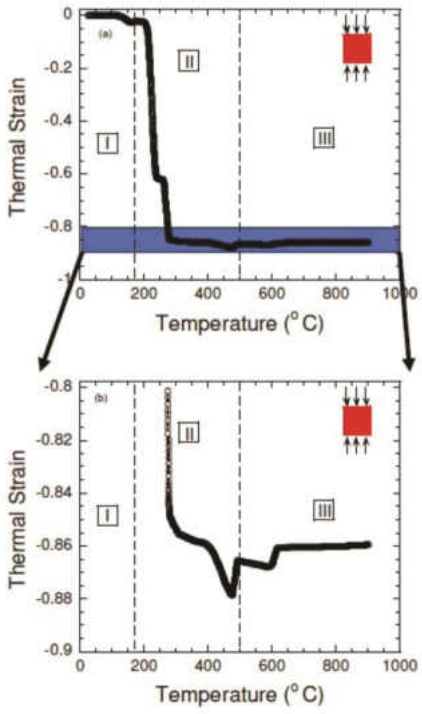

Figure 2.9: TMA measurement of pure Lignin (*this image is used from the ref.* [5] *for criticism under fair usage*).

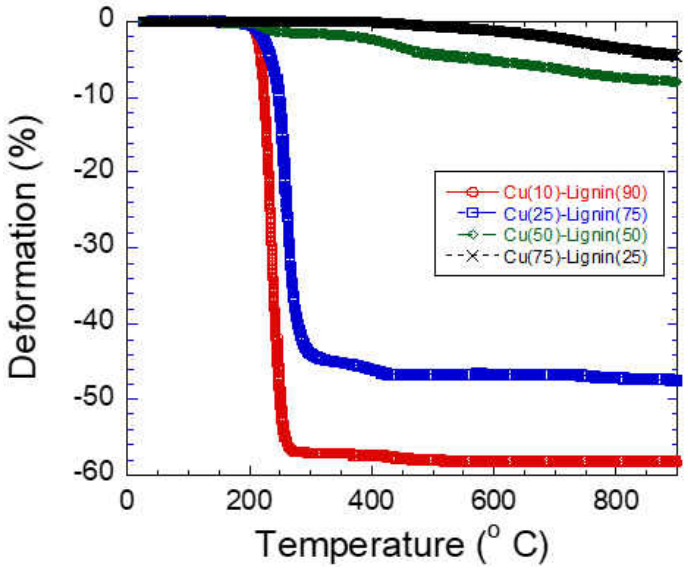

Figure 2.10: TMA measurements of Cu-Lignin composites.

The Type-I composites, for example Cu(10)-Lignin(90) and Cu(25)-Lignin(75), show thermomechanical behavior like lignin where the sample considerably between 200-300 ºC, thereafter the deformation slows down. Comparatively, the overall deformation of these composites is lower than pure lignin (~86% deformation, Fig. 2.9) which indicates that Cu is reinforcing the matrix and decreasing the deformation of the matrix. Comparatively, Type-II composites had significantly lower deformation than type-I composites which indicate that the Cu matrix is able to support the matrix although lignin is pyrolytically decomposing.

2.3.5 Mechanical Behavior

Figure 2.11 shows the stress versus displacement plots for each composite system during compression testing. Typical mechanical behavior for brittle foams is observed for Type-I composites across all fabrication temperatures. The behavior includes several failures of small links/cell walls within the structure before seeing strength enhancement. This cycle continues until a maximum stress, often the absolute maximum, causes catastrophic failure within the structure.

While 10% volume addition of copper is observed to yield well behaved porous structures, the strength of the foams is maintained at 1-2 MPa. However, the addition of 25 vol. % of copper does result in a significant increase of compression strength, ranging from 5-9 MPa. Such behavior was also observed for pure lignin carbon foams [5].

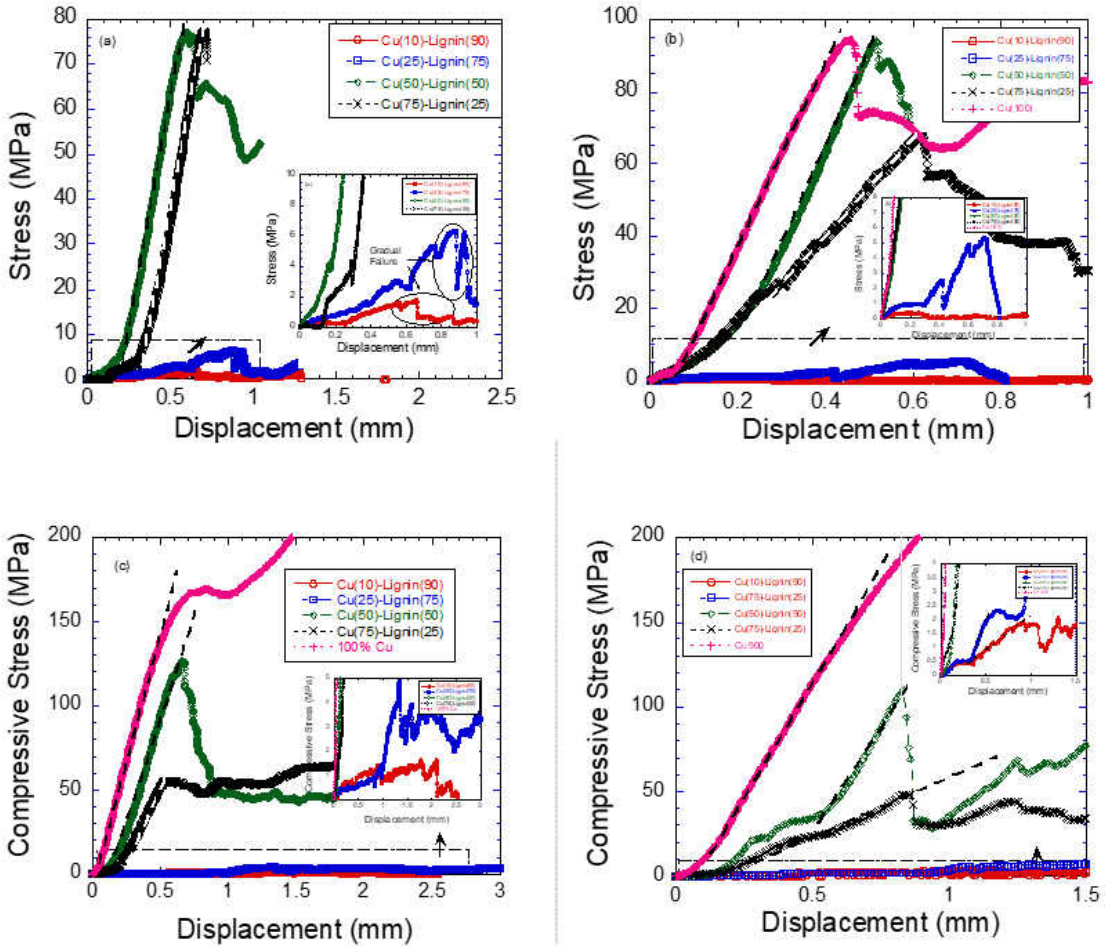

Figure 2.11: Plot of compressive stress versus displacement of Cu-Lignin composites pyrolyzed at, (a) 300 ºC, (b) 500 ºC, (c) 700 ºC, and (d) 900 ºC.

Comparatively, Type-II composites showed similar behavior as pure Cu. Pure Cu was brittle at 300 ºC, and could not be tested as the samples crumbled during the machining process,

however as the sintering temperature was increased, we observed an enhancement in compressive strength at 500 and 700 ºC, respectively (Fig. 2.12a). The fabrication temperature also has strong influence on the strength of Type-II composites, however, where we see a wider range of strengths for each composition.

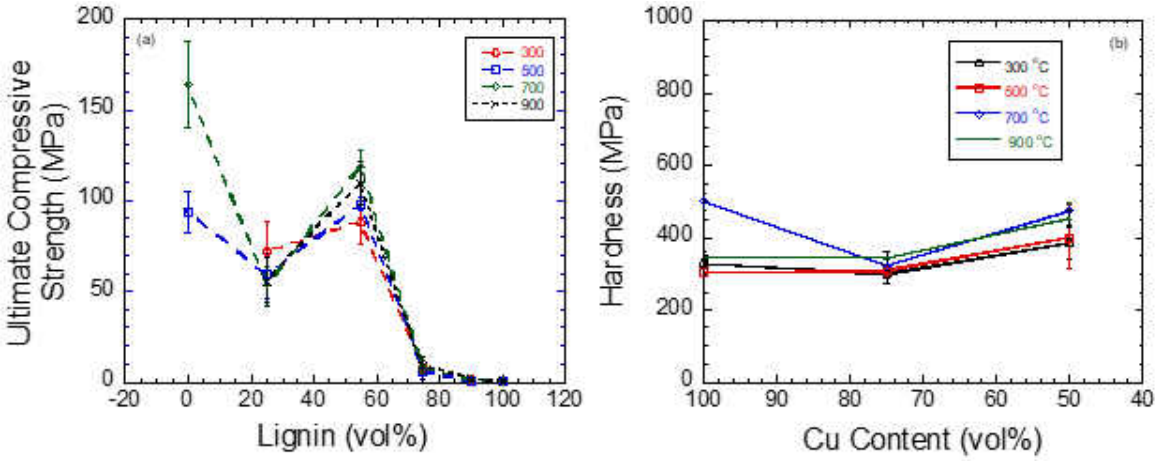

Figure 2.12: Plot of, (a) UCS and (b) hardness of Cu-Lignin composites.

As compared to pure Cu which was like a biscuit at 300 ºC and could not be tested, Cu(75)-Lignin(25) and Cu(50)-Lignin(50) had UCS of ~72 and ~88 MPa, respectively. At 500 ºC, the UCS of Cu was ~94 MPa as compared to ~59 and ~98 MPa in Cu(75)-Lignin(25) and Cu(50)-Lignin(50), respectively. This study shows that lignin can be a potential binding phase for cementing Cu particles in the 300-500 ºC range as compared to pressureless sintering of Cu-particles as the densification and sintering process in pure Cu is negligible in this temperature range. However, after heat treatment at 700 ºC, the UCS of Cu was ~163.5 MPa as compared to ~54 and ~119 MPa in Cu(75)-Lignin(25) and Cu(50)-Lignin(50), respectively. Similarly, at 900

°C, Cu showed ductile failure, and Cu(75)-Lignin(25) and Cu(50)-Lignin(50) fractured in a brittle manner, and had UCS of ~55.5 and ~110 MPa, respectively. In this regime, the sintering of Cu particles has become active, and pure Cu compacts perform better than the Cu-Lignin compacts. Nevertheless, Cu(50)-Lignin(50) showed UCS >100 MPa at both 700 and 900 °C, respectively. On closer inspection, we also observed that Cu(50)-Lignin(50) had higher UCS than the other Cu-Lignin compositions (Fig. 2.12a). This indicates that 50 vol% lignin is optimum concentration to bond Cu particles. The hardness measurements also showed similar correlation were the addition of lignin increased the hardness of the compacts which further support the argument that lignin can be used for cementing Cu particulates (Fig. 2.12 b)

2.3.6 Wettability

To continue the investigation into wettability tailoring by fabrication temperature adjustment, the wettability behavior is summarized in Fig. 2.12. In this thesis, we will use the definition proposed by Law [9], where hydrophobic surface is defined as contact angle >90°, and hydrophilic surface is defined as those surfaces where contact angle is <90°. As observed from the plot, Cu has contact angle of 86.5°, 89.0°, 93.4°, and 94.7° after treatment at 300, 500, 700, and 900 °C, respectively which is indicative of the hydrophobic nature of the surface. This behavior of Cu strongly influences the wettability of the Type-II composite systems, which don't see as strong temperature dependency as Type-II composites. In general Type-I composites show similar temperature dependent wettability of pure pyrolyzed lignin [5] where compositions fabricated at 300 and 500 °C are hydrophobic, and compositions fabricated at 700 and 900 °C are hydrophilic. One exception is found, where Cu-L 25%-75% is found to be hydrophilic despite being fabricated at 500 °C. Clearly, by adding Cu in the lignin matrix, we can diversify and engineer the wettability of Cu-Lignin foams.

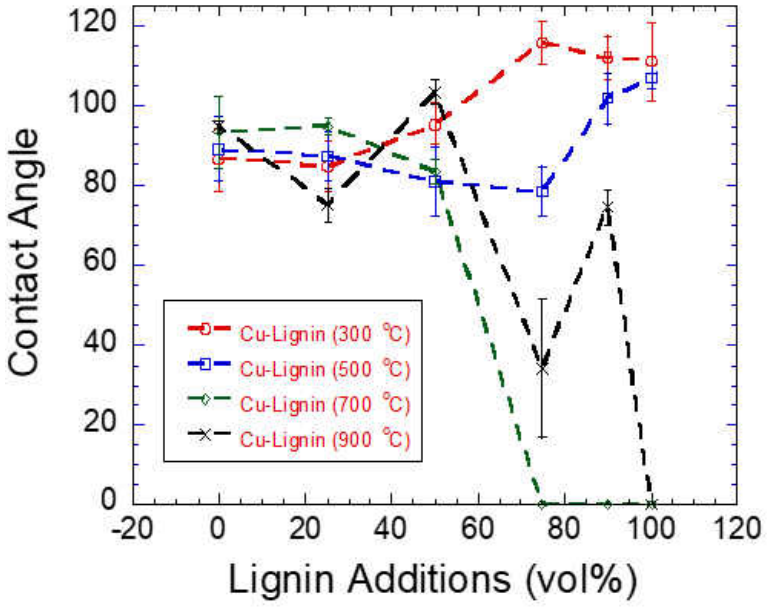

Figure 2.13: Wettability behavior of different Cu-Lignin composites.

2.3.7 Comparison with Cu foams

Sharma et al. [10] fabricated Cu foams used acrawax as pore formers and designed foams with 40-70 vol% porosity. They used a two-step sintering process where they performed debinding at 350 °C for 2h, followed by sintering at 900 °C for 60 min in Ar atmosphere. They reported a yield strength of 4 MPa for 70% porous samples. Zhao et al. [11] designed Cu foams with a porosity of 50-85% by using K_2CO_3 as pore former. They sintered their samples at 850 °C for 4 h and subsequent removal of carbonate by cooling the compacts and dissolving in water or further heat treatment at 950 °C to remove the carbonate. All the samples showed yielding behavior during mechanical testing. In our study, we showed that it is possible to design porous compacts by using a single step manufacturing process to synthesize Type-I and Type-II composites. Comparatively, Lignin(75)-Cu(25) compositions had porosity of ~67.2, ~67.1, ~69.6, and ~68.4%, after pyrolysis at 300, 500, 700, and 900 °C, respectively. The UCS of these composites were in the range of 5-9

MPa. Although, the type-I foams which we designed are pyrolyzed lignin matrix reinforced with Cu particulates, they still favor comparably with Cu-based foams. From sintering perspective, Babu and Kanagaraj [12] observed that addition of carbon-based material like Carbon Nano Tubes (CNT) interfere with the sintering of Cu-matrix except 0.25 wt. % CNT addition where enhancement in relative density was observed. There is a critical requirement for electrically conductive light material [13] . This study shows lignin can effectively sinter Cu thus further studies should be conducted for understanding the electrical behavior of type-I and II composites.

2.3.8 Conclusions

Cu was successfully used as both a particulate inclusion and a matrix, Type I and II composites, respectively. As proposed by our hypothesis, Cu additions enhanced the strength of Type-I composites from a pure lignin-based foam. Type-I composites also maintain lignin's temperature-sensitive wettability, exhibiting hydrophobic behavior for fabrication at 300 and 500 °C, respectively and hydrophilic behavior for fabrication at 700 and 900 °C, respectively.

In Type-II composites, we observed for the first time that lignin can be used as a sintering aid and can cement Cu-particulates. For example, Cu-Lignin composites fabricated at 300 °C showed higher strength than pure Cu which is indicate of the cementing behavior of lignin. Thus, lignin can be used as a low temperature sintering aid and binder for copper composites. In addition, the wettability of lignin foams can be controlled by making composites with Cu.

CHAPTER 3: SYNTHESIS AND CHARACTERIZATION OF DDGS – LIGNIN COMPOSITES

3.1 Introduction

In a separate study, investigation into the reutilization of byproducts from biomass is expanded to include distiller's dried grains with solubles (DDGS). The material is specifically the waste product of the extraction of ethanol from corn. While DDGS can include waste material from other plant sources, here it is used to specifically describe that of corn. For example, if 1 Kg of processed corn can lead to equal proportion of ethanol, DDGS, and CO_2 (1/3 Kg yield of each constituent) [14] . Chemically DDGS is composed of protein (33%), fat (8.71%), cellulose (13.2%), hemicellulose (30%), and 2% lignin (see Table 3, Ref. [15]), and is non-fermentable portion of the original grain [14]. DDGS has low cost of 8-13 cent per Kg [15]. It is predominantly used as animal feed [16]. If we can use DDGS for high-end materials design, then we can increase the valuation of materials further. Cheesbrough et al. [14] have summarized that DDGS has excellent potential as resin glue composites. Liaw et al. [15] have shown that DDGS is effective as natural adhesive for particle boards. Reimar et al. [17] have designed supercapitors by using DDGS. Zarrinbaksch et al. [18] observed similar properties as polypropylene (PP) matrix in a blend composed 10 wt. % DDGS, 2.4 wt. % maleated PP (PPgMA), 2.2 wt% maleated ethylene-propylene-diene monomer rubber (EPDMgMA) and rest PP. Tisserat et al. [19] fabricated composite wood panels by making composites of DDGS with eastern redcedar. In a later study, Tisserat et al. [20] designed bio-based wood panel by using 50% DDGS and 50% Prosante soybean flours as the cementing matrix which were further reinforced pinewood. In this chapter, we will document the use of DDGS for fabricating biofoams.

3.2 Experimental Details

3.2.1 Design Paradigm

DDGS was procured from a local plant (Theraldson Ethanol, Casselton, ND). The as-received were dried at 100 ^{o}C for 24 h. These powders were then ball milled (8000 M mixer Mill, SPEX SamplePrep, Metuchen, NJ) for 60 min. Lignin (Indulin AT, MeadWestvaco, Richmond, VA) and milled DDGS were ball milled to mix the powders for 5 mins. The following weight fractions were used during this study: (a) 90% DDGS - 10% lignin (DDGS(90)-L(10)), (b) 75% DDGS - 25% lignin (DDGS(75)-L(25)), (c) 50% DDGS -50% lignin (DDGS(50)-L(50)), and (d) 25% DDGS - 75% lignin (DDGS(25)-L(75)).

3.2.2 Fabrication Process

DDGS and lignin powders are first combined with the respective mass fractions and ball milled for 5 min in a ball mill (8000 M mixer Mill, SPEX SamplePrep, Metuchen, NJ). Please refer to the last chapter regarding the pellet fabrication procedure. In this study, we used a 10 ton hydraulic press instead of Carver press in the last chapter for cold pressing samples, but all the other conditions were same. The green bodies were then placed in a tube furnace in flowing Ar atmosphere. To further decrease the probability of oxidization, Ti powders were placed at each end of the furnace, adjacent to the seals. All the compositions were pyrolyzed at 300 and 900 ^{o}C for 1 h after heating at 10 ^{o}C /min to the desired temperature. The sample is removed from the furnace once the furnace temperature reaches below 100 ^{o}C.

3.2.3 Sample Characterization

3.2.3.1 Microstructure Analysis

Please refer to Chapter 2 regarding the details of surface preparation and SEM characterization. X-ray tomography was performed by using the analysis described in ref. [8].

3.2.3.2 Porosity Analysis

Please refer to Chapter 2 regarding the details on protocol of porosity analysis.

3.2.3.3 Thermomechanical Analysis (TMA) and Thermogravimetric Analysis (TGA)

Please refer to Chapter 2 regarding the protocol of TMA. The weight loss kinetics of DDGS during pyrolysis was monitored by using a thermogravimetric analyzer (TGA Q500, TA Instruments, New Castle, DE). During this study, a few mgs of DDGS samples heated at a heating rate of 10 °C/min until 950 °C in N_2 atmosphere.

3.2.3.4 Fourier-Transform Infrared Spectroscopy (FTIR)

Please refer to Chapter 2 regarding the protocol of FTIR analysis.

3.2.3.5 Compression Testing

Please refer to Chapter 2 regarding the protocol for compression testing.

3.2.3.6 Contact Angle Measurement (Wettability Analysis)

Please refer to Chapter 2 regarding the protocol for wettability analysis.

3.3 Results and Discussion

3.3.1 Analysis of DDGS Powders

Figures 3.1a and b shows the microstructure of DDGS particles. Table 3.1 shows the EDS reading of different regions. In general, DDGS particles are irregular shaped. Figures 3.1c and 3.1d

show the powders after treatment at 300 and 900 ^{o}C, respectively. In general, particles retained similar shape but agglomeration of particles due to pyrolysis was observed.

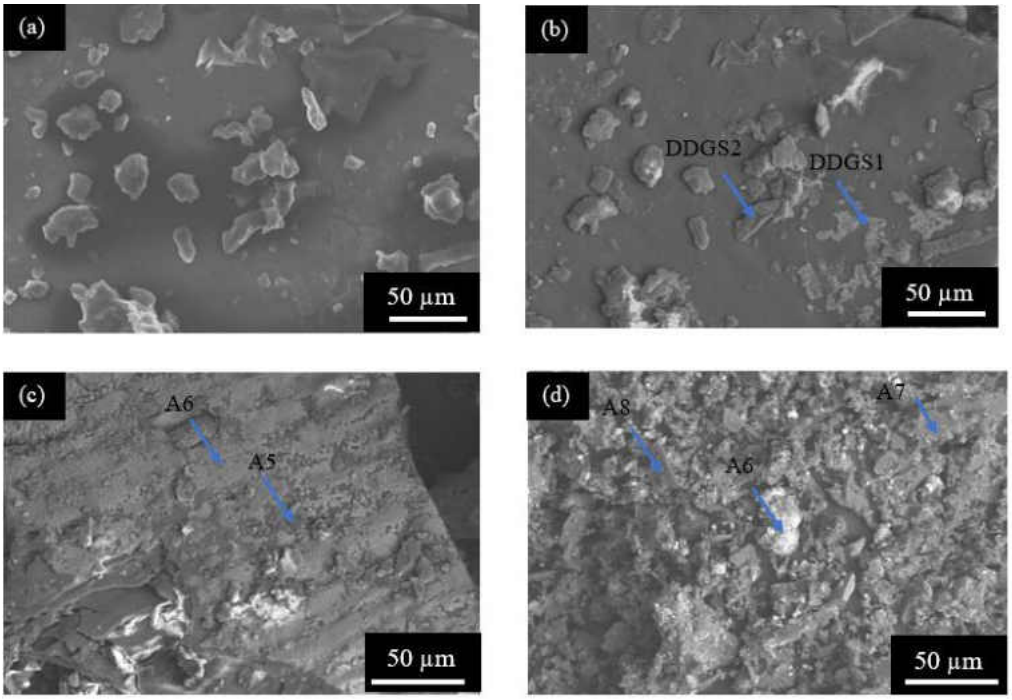

Figure 3.1: SEM micrographs of powders of, (a) DDGS in SE, (b) BSE of the same region, and DDGS pyrolyzed at, (c) 300 ^{o}C, and (d) 900 ^{o}C.

Figure 3.2 shows the TGA behavior of different biomass. DDGS also shows similar behavior. Currently, Dr. Gupta's team is performing chemical analysis of these precursors so that we can have a holistic understanding of different biomass.

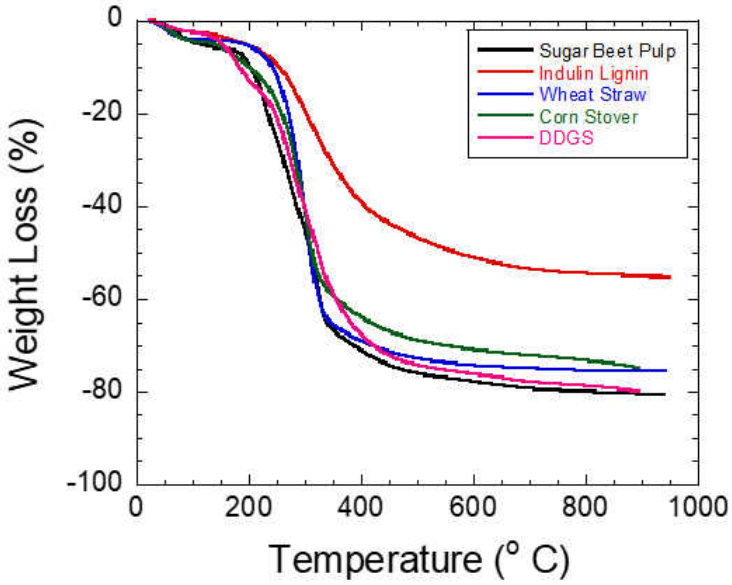

Figure 3.2: TGA behavior of biomass.

Table 3.1: EDS Analysis of PoI

Composition	C-K	O-K	Na-K	Mg-K	Si-K	P-K	S-K	Cl-K	K-K	Ca-K	Al	Zr
DDGS1	36.4±5.51	47.1±1.92	2.93±0.07	2.05±0.33	0.2±0.01	2.53±0.46	3.51±0.39	0.33±0.07	5.98±0.33	x		
DDGS2	54.6±3.35	39.1±4.01	2.93±0.07	0.60±0.12	0.24±0.02	0.77±0.12	0.50±0.08	0.27±0.06	1.69±0.04	1.46±0.27		
A5	70±23.97	28±1.08	0.53±0.11	0.60±0.15	x				0.83±0.26	x		
A6	23.4±0.65	52.1±1.01	5.67±0.30	1.04±0.16	x	0.52±0.03	5.56±0.20	x	11.5±0.95			
A7	36.7±0.4	34.5±0.28	0.55±0.05	1.54±0.05	5.68±0.20	1.38±0.03	2.52±0.01		3.03±0.05	14.0±0.17	x	
A8	50.5±1.39	17.5±1.12	1.00±0.12	1.98±0.03	0.59	8.17±0.21	1.12	0.86	19.2±0.16	x		
A9	94.5±0.15	0	0.94±0.01	0.53±0.03		1.16±0.03	0.48	0.25±0.03	2.29±0.04			
DDGS300	42.6±0.55	40.5±1.45	0.94±0.04	0.52±0.05			0.19±0.07		0.63±0.04	0.49±0.30	0.21±0.02	0.60±0.03
A13	46±3.92	35.4±0.92	2.02±0.53		x		2±0.58		13.3±2.17		1.4±0.24	
A14	56.1±2.56	32.6±1.06	1.38±0.28	0.68±0.41		x			4.54±0.52	3.76±1.53	0.97±0.31	
A15	69±2.27	26.9±3.53	0.94±0.29				x		0.68±0.59	0.39±0.21		
A16	61±0.84	18.6±1.83	0.60±0.10	0.43±0.27	8.36±0.84				4.78±0.41	1.72±0.25	4.50±0.61	
A17	45.4±1.53	34.1±0.78	0.86±0.30						4.25±0.53			
DDGS9001	93.4±0.13	x	1.07±0.02	1.64±0.04		1.91±0.01	0.19±0.02	x	1.75±0.13			x
DDGS9002	95.2±0.1	x	1.21±0.05	1.06±0.03		1.38±0.05			1.18±0.06			
DDGS9003	30.8±1.62	55.7±1.84	0.56±0.05	1.04±0.1		0.96±0.15			10.8±0.08	x		
A18	83.4±16	27.8	1.43±0.15				x		5.88±0.16			
A19	79.2±11	19.3±0.20	1.97±0.05	1.63±0.06	x	1.95±0.1			2.36±0.29			
A20	67.4±0.27	24.7±0.41	1.71±0.14				0.55±0.03		5.7±0.25			
A21	97.1±0.09	x	1.15±0.03	x		x	0.62±0.09		1.10±0.10			
A22	41.8±3.71	41.8±3.11	14.2±1				0.90±0.21		1.28±0.19			

3.3.2 Microstructure Analysis of Pyrolyzed Foams

Figure 3.3 shows the microstructures of different compositions of DDGS-Lignin pyrolyzed at 300 ºC. The DDGS pyrolyzed at 300 ºC shows agglomerated cores of DDGS separated by pores and fissures (Figs. 3a,b). This shows that DDGS by itself cannot form a well-connected porous biofoam. DDGS(90)-Lignin(10) also showed similar features where agglomerated regions of DDGS were separated by cracks and fissure were observed (Fig. 3c). The addition of higher wt. % of lignin helped in cementing DDGS particles in DDGS(75)-Lignin(25) and DDGS(50)-Lignin(50) compositions (Figs. 3d-f). Comparatively, DDGS(25)-Lignin(75) showed cellular microstructure like observed in pyrolyzed lignin compacts [5]. Figure 3.4 shows the microstructure of DDGS-Lignin composites pyrolyzed at 900 ºC. The microstructure of DDGS-lignin composites showed similar trend as the composites fabricated at 300 ºC. Essentially, the DDGS compacts are composed of disjointed and agglomerated pyrolyzed DDGS particles (Fig. 3.4 a-b). DDGS(90)-Lignin(10) also showed similar microstructure which indicates that lignin is insufficient to bind the particles together (Figs. 3.4 c-d). The addition of higher wt. % of lignin aids in cementing the lignin particulates in DDGS(75)-Lignin(25) (Figs.3.4 e-f). In this composition, mineral-rich cementing nodules were also observed (A19, Table 3.1). This may have formed due to reaction of lignin with mineral rich constituents of DDGS. Comparatively, DDGS(50)-Lignin(50) (Figs. 3.4 g-h) and DDGS(27)-Lignin(25) (Fig. 3.4 i-j) showed cellular microstructure like pyrolyzed lignin compacts [5].

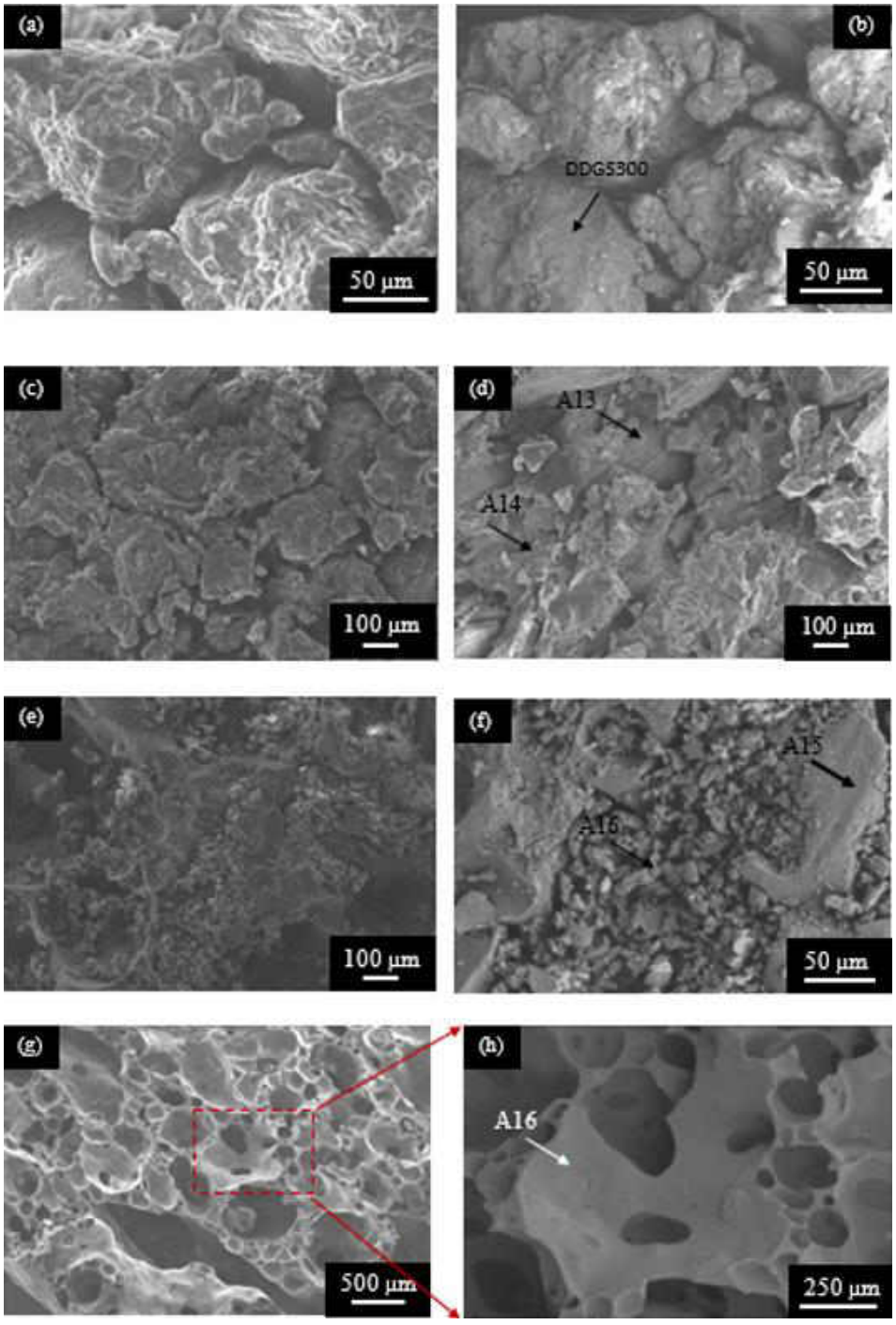

Figure 3.3: SEM micrographs of sintered compacts of, (a) DDGS(300 ^{o}C) in SE, (b) BSE of the same region, (c) DDGS(90)-Lignin(10)(300 ^{o}C) , (d) DDGS(75)-Lignin(25)(300 ^{o}C) , (e) DDGS(50)-Lignin(50)(300 ^{o}C) , (f) BSE of the same region, (g) DDGS(25)-Lignin(75)(300 ^{o}C), and (h) BSE of the same region.

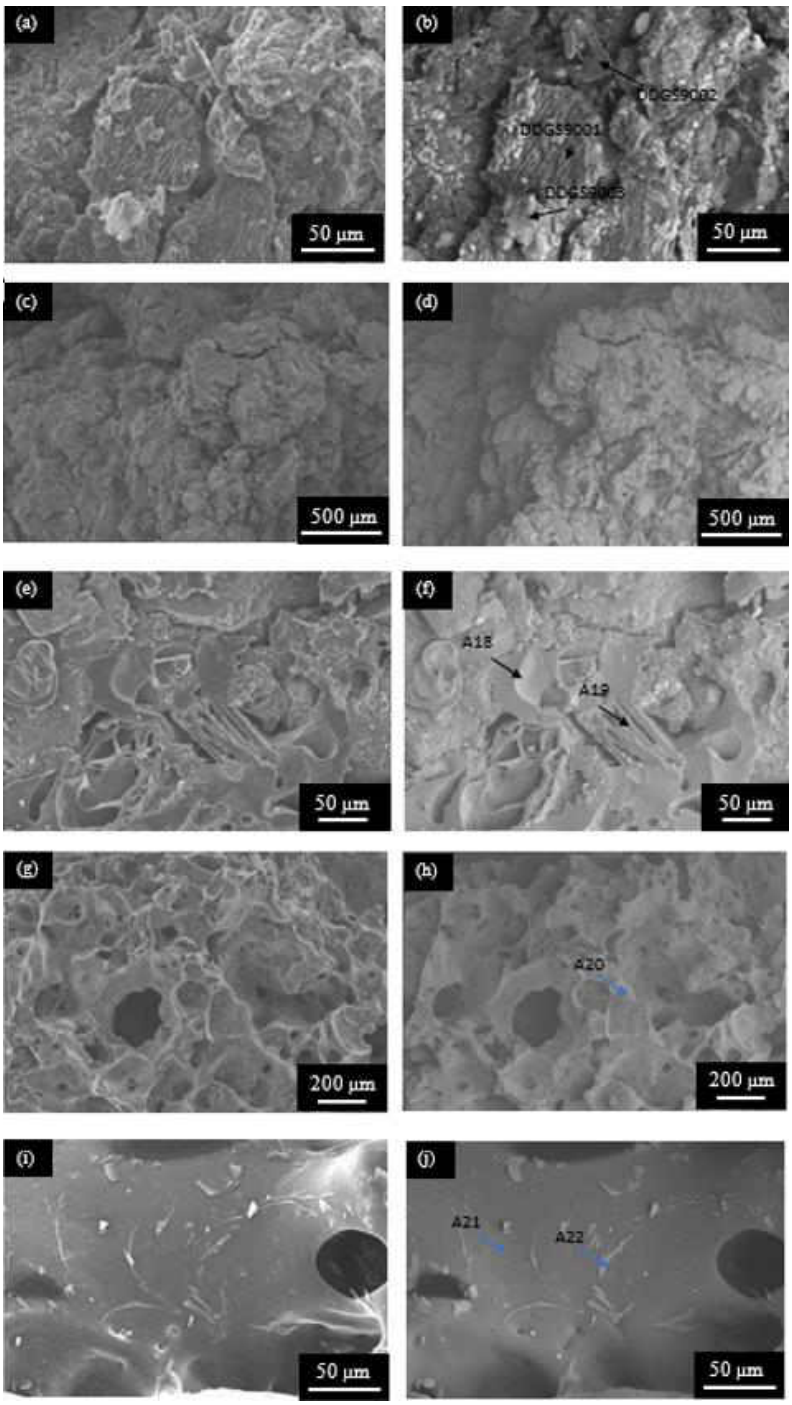

Figure 3.4: SEM micrographs of sintered compacts of, (a) DDGS (900 ºC) in SE, (b) BSE of the same region, (c) DDGS(90)-Lignin(10)(900 ºC), (d) BSE of the same region, (e) DDGS(75)-Lignin(25)(900 ºC), (f) BSE of the same region, (g) DDGS(50)-Lignin(50)(900 ºC), (h) BSE of the same region, (i) DDGS(25)-Lignin(75)(900 ºC), and (j) BSE image of the same region.

3.3.3 Porosity

Figure 3.5 shows the plot of porosity versus lignin additions. DDGS pyrolyzed at 300 and 900 ^{o}C have porosity of ~46 and ~62%, respectively. The addition of 10 and 25 wt. % lignin reduced the porosity to ~36 and 41.5%, respectively after pyrolysis at 300 ^{o}C; the porosity after the addition of 10 and 25 wt. % lignin further increased to 51.2% and 50%, respectively after pyrolysis at 900 ^{o}C. Like it was observed in the microstructure studies, these results show that lignin can be binding agent to cement DDGS particulates during pyrolysis. However, after additions of 50 and 75 wt. % lignin, the porosity increased to ~74 and ~88%, respectively, after pyrolysis at 300 ^{o}C; the porosity increased to ~87 and ~92%, respectively after pyrolysis at 900 ^{o}C. Comparatively, pure lignin had porosity of ~93% and ~93.4% after pyrolysis at 300 and 900 ^{o}C, respectively. This shows that synergistically, lignin-DDGS biofoams can generate similar porosity as pyrolyzed lignin compacts [5].

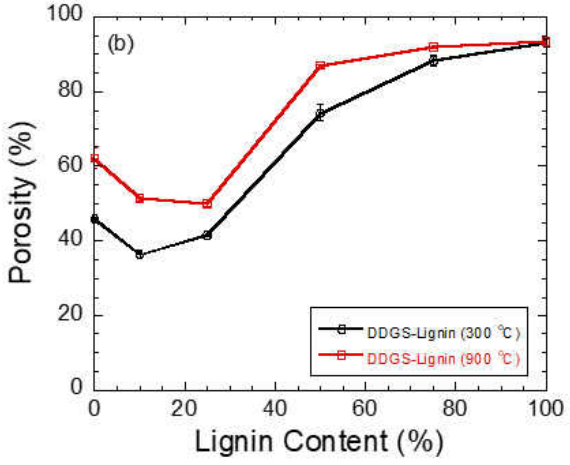

Figure 3.5: Plot of porosity vs. lignin addition for DDGS-Lignin composites fabricated at 300 °C and 900 °C.

3.3.4 TMA

The thermomechanical behavior of the composite systems is plotted in Fig. 3.6. Similar to lignin matrices, the DDGS matrices liquify during pyrolysis when heated beyond 200 °C, thereafter it solidifies by 300 °C. During temperature, lignin-DDGS compact also deforms significantly. The addition of DDGS in lignin decreases the overall deformation as DDGS particles can constrain the deformation of DDGS-lignin compacts.

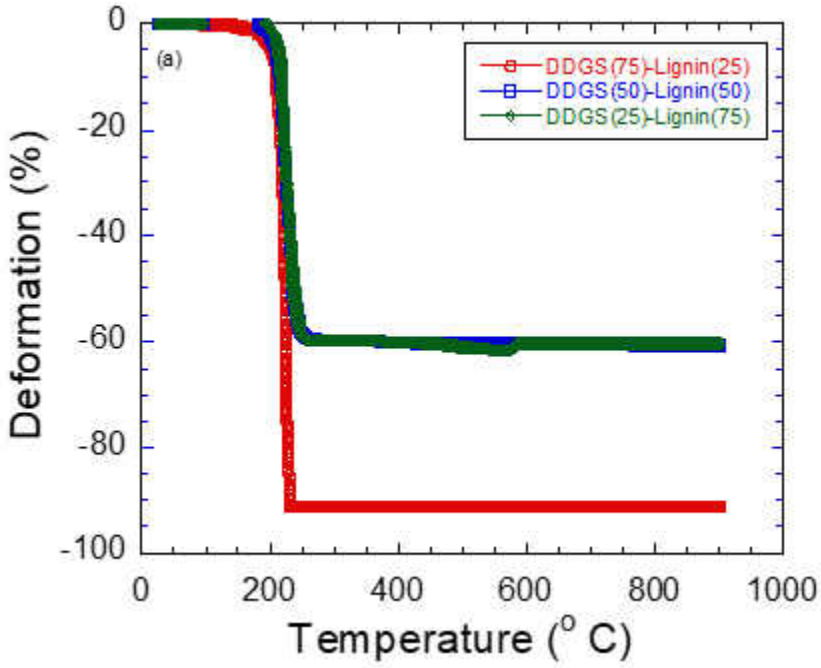

Figure 3.6: TMA of DDGS-Lignin composites.

3.3.5 FTIR

Figure 3.7 shows the FTIR analysis for pure DDGS, pure lignin, and their composites. We can observe that the intensity of peaks decreased after pyrolysis at 900 °C as compared to the data after 300 °C. This indicates that DDGS-Lignin compacts are decomposing at higher temperatures. This fact was also observed during TGA analysis (Fig. 3.2). Currently, we are in

the process of completing chemical analysis of DDGS. Once it is completed, we will be able to index the peaks. The results will be published in follow up publication.

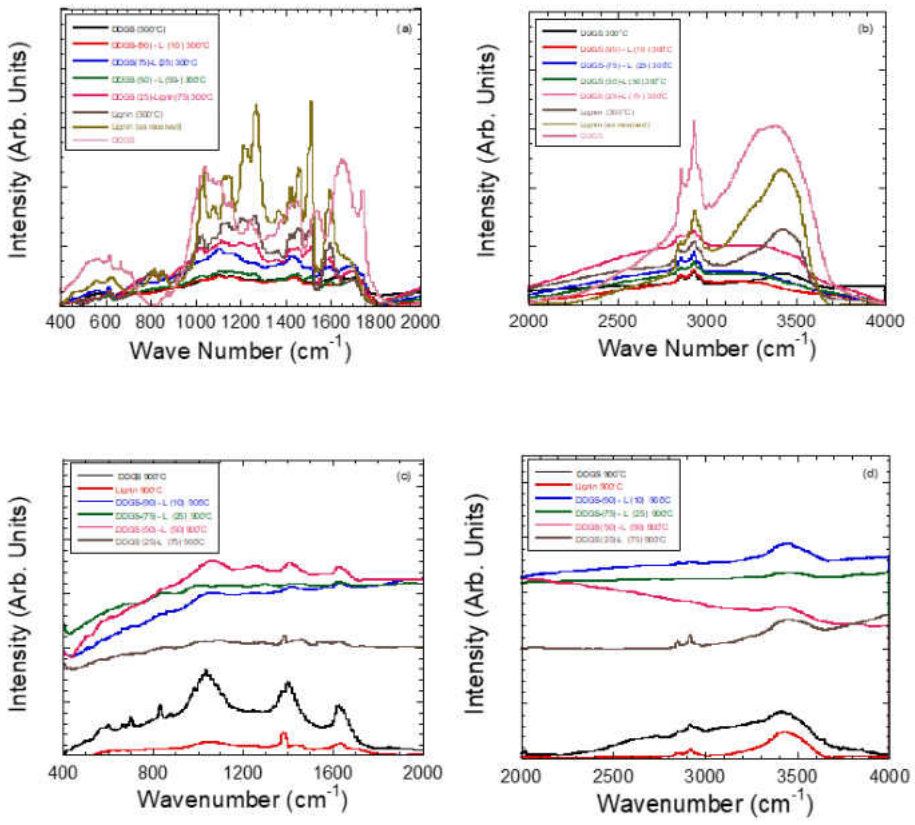

Figure 3.7: FTIR of Lignin-DDGS composites after pyrolysis at, (a) 300 ºC (400-2000 cm^{-1}), (b) 300 ºC (2000-4000 cm^{-1}), (c) 900 ºC (400-2000 cm^{-1}), and (d) 900 ºC (2000-4000 cm^{-1}).

3.3.6 X-ray Tomography

X-ray images for DDGS-Lignin compositions fabricated at 300 °C and 900 °C are presented in Figures 3.8 and 3.9, respectively. DDGS(90)-Lignin(10) and DDGS(75)-Lignin(25) after pyrolysis at 300 ºC (Figs. 3.9 a1-a4 and b1-b4) and 900 ºC (Figs. 3.9 a1-a4 and b1-b4) showed denser morphology where no macropores were observed which is indicative of the low porosity of DDGS as lignin is acting as cementing agent in these composites. This fact is also supported by porosity analysis (see section 3.3.3).

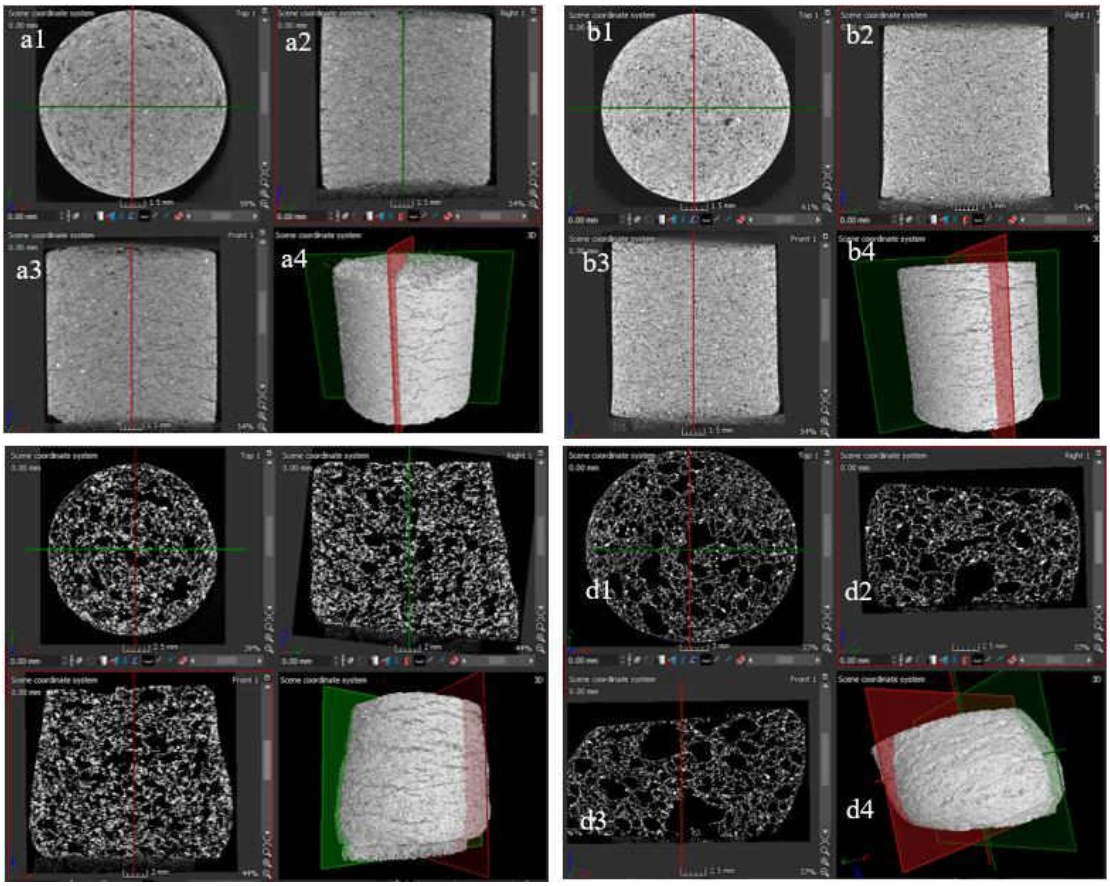

Figure 3.8: X-ray tomography images of, (a1) DDGS(90)-Lignin(10) (cross-section), (a2-a3) side views, and (a4) morphology of the entire sample; (b1) DDGS(75)-Lignin(25) (cross-section), (b2-b3) side views, and (b4) morphology of the entire sample; (c1) DDGS(50)-Lignin(50) (cross-section), (c2-c3) side views, and (c4) morphology of the entire sample; and (d1) DDGS(25)-Lignin(75) (cross-section), (b2-b3) side views, and (b4) morphology of the entire sample after pyrolysis at 300 ^{o}C for 1h.

Comparatively, DDGS(50)-Lignin(50) (Figs. 3.8 c1-c4 and 3.9 c1-c4) and DDGS(25)-Lignin(75) (Figs. 3.8 d1-d4 and 3.9 d1-d4) showed cellular microstructures. However, we could not see large cavity defects as observed during pyrolysis of lignin compacts [5]. These studies show that lignin-DDGS offers us unique material options for designing composites with tailored porosity.

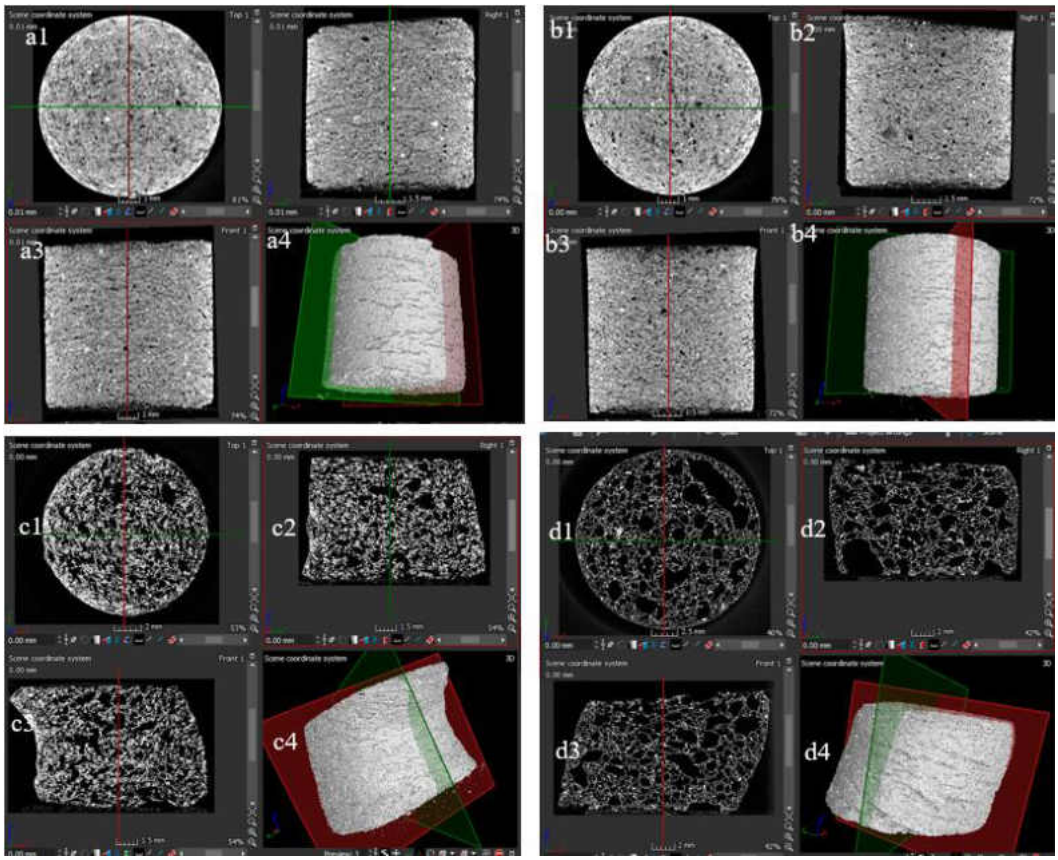

Figure 3.9: X-ray tomography images of, (a1) DDGS(90)-Lignin(10) (cross-section), (a2-a3) side views, and (a4) morphology of the entire sample; (b1) DDGS(75)-Lignin(25) (cross-section), (b2-b3) side views, and (b4) morphology of the entire sample; (c1) DDGS(50)-Lignin(50) (cross-section), (c2-c3) side views, and (c4) morphology of the entire sample; and (d1) DDGS(25)-Lignin(75) (cross-section), (b2-b3) side views, and (b4) morphology of the entire sample after pyrolysis at 900 ^{o}C for 1h.

3.3.7 Compression Testing

The mechanical strength and behavior of the composite systems are shown in Fig. 3.10.

All the compositions showed a combination of gradual and brittle failure (Fig. 3.10a and b).

DDGS pyrolyzed at 300 and 900 °C had UCS of ~1.75 and ~7.56 MPa, respectively as compared to ~0.75 and ~0.95 MPa in lignin after pyrolysis at 300 and 900 °C, respectively [5].

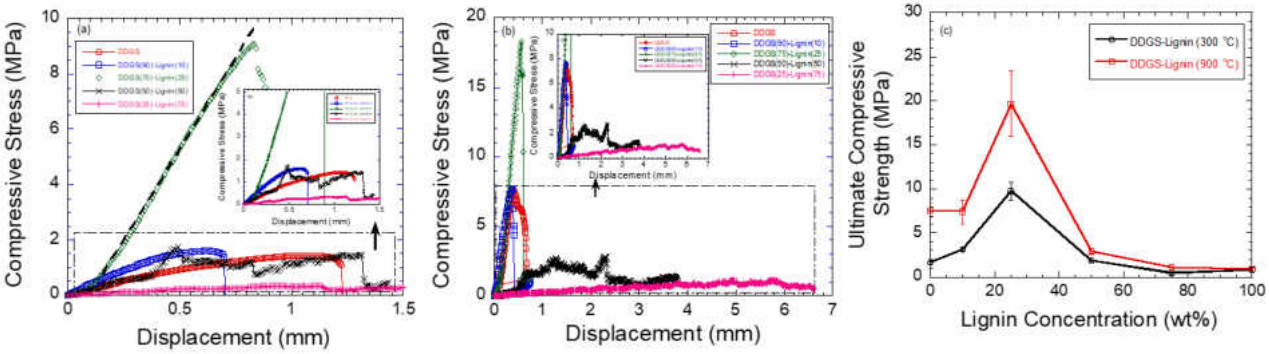

Figure 3.10: Plot of compressive stress versus displacement of Lignin-DDGS composites pyrolyzed at, (a) 300 °C, (b) 900 °C, and (c) UCS versus lignin concentration in DDGS-Lignin composites.

Interestingly, the addition of 10 wt. % lignin in DDGS matrix improved the UCS to ~3.12 and ~7.40 MPa after pyrolysis at 300 and 900 °C, respectively. Comparatively, the addition of 25 wt. % lignin enhanced the UCS further to ~9.8 and ~19.7 MPa, respectively. Thereafter, the addition of 50 wt. % of lignin decreased the UCS to ~1.88 and ~2.96 MPa, respectively after pyrolysis at 300 and 900 °C. Comparably, after the additions of 10 and 25 wt. % lignin, the porosity reduced to ~36 and 41.5%, respectively after pyrolysis at 300 °C; the porosity after the addition of 10 and 25 wt. % lignin further increased to 51.2% and 50%, respectively after pyrolysis at 900 °C. At higher lignin content, DDGS(50)-lignin(50) had UCS of ~1.88 (porosity - ~74.3%; bulk density (BD) - ~0.37 g/cc) and ~2.96 MPa (porosity - ~86.9%; bulk density – 0.31 g/cc) after pyrolysis at 300 °C, and 900 °C, respectively. The UCS further decreased to ~0.47 and ~1.10 MPa after the addition of 75 wt. % lignin, and subsequent pyrolysis at 300 and 900 °C, respectively.

By analyzing the results, we can conclude that 25 wt. % lignin is optimal addition to enhance the performance of DDGS-lignin compacts where lignin is acting as a cementitious

bonding phase but it is not creating a network of macropores which can lower the strength of the composites. For comparison, Carbon-foam fabrication is pyrolysis route is tedious as it involves, heating and pressurization, subsequent depressurization, and carbonization [21]. For example, Eksilioglu et al. [21] used naphthalene-based mesophase pitch with a softening point of 556 K to design porous foams. During this process, they process the compacts the inert N_2 atmosphere at 553, 556, 566 and 573 K at 6.8 MPa constant pressure and 5 s release time. The porosity varied in these samples from 44.9 to 80.6%, and compressive strength varied between 1.47 and 3.31 MPa as the temperature was changed from 553 to 573 K. Lignin-DDGS compositions compare favorably with these results. Due to the use of biobased precursors, we can use agricultural precursors for this research. In addition, the process used in this research does not need any autoclave for pressurization hence we potentially use this process for continuous production of foams.

3.3.8 Wettability

Figures 3.11 and 3.12 show the contact angle measurements for compositions fabricated at 300 °C. The compositions DDGS(90)-Lignin(10), DDGS(75)-Lignin(25), DDGS(50)-Lignin(50), and DDGS(25)-Lignin(75) after pyrolysis at 300 °C were hydrophobic as compared to DDGS(90)-Lignin(10) which was hydrophilic.

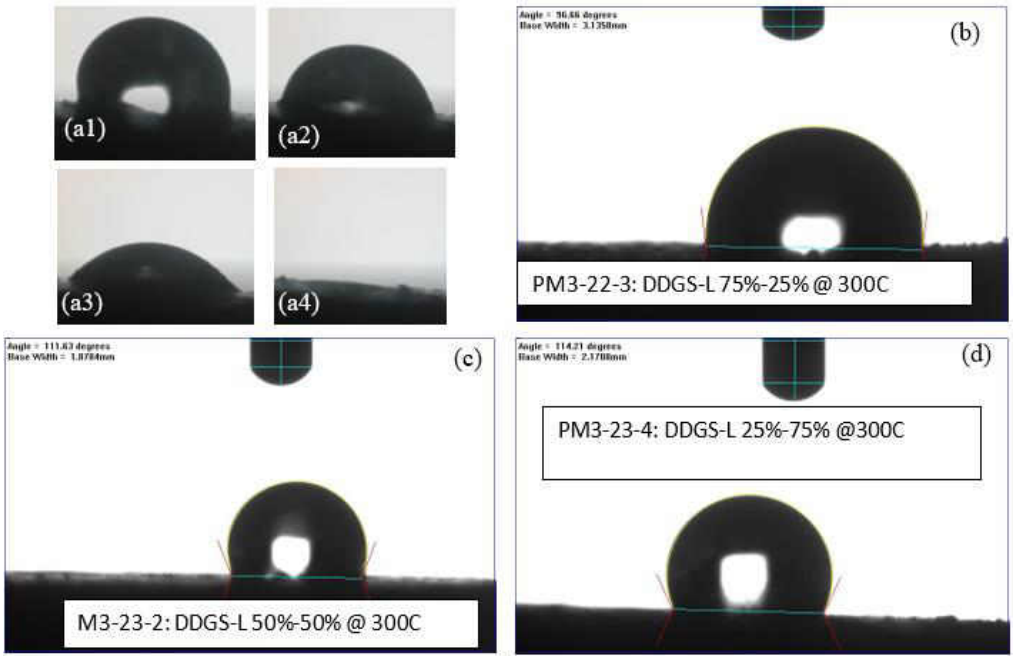

Figure 3.11: Wettability of, (a) DDGS(90)-Lignin(10), (b) DDGS(75)-Lignin(25), (c) DDGS(50)-Lignin(50), and (d) DDGS(25)-Lignin(75) at 300 °C.

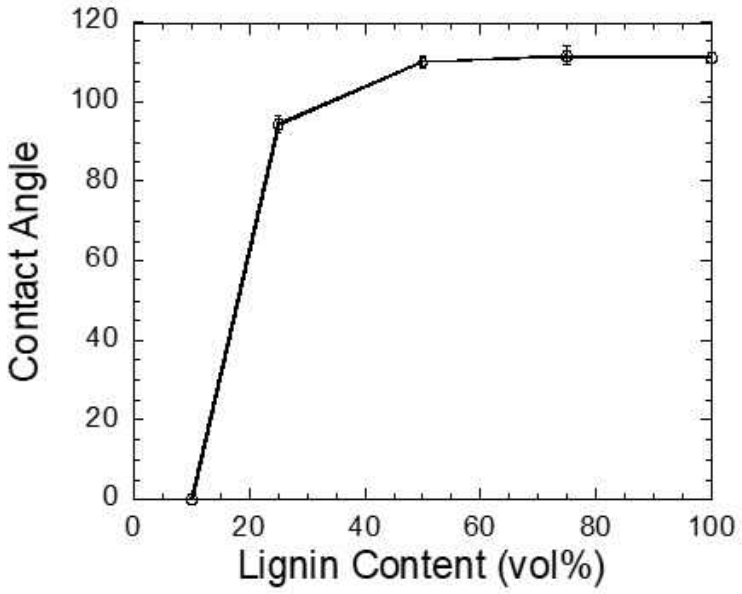

Figure 3.12: Contact angle measurements of DDGS-lignin composites.

All the compositions fabricated at 900 °C were hydrophilic in nature.

3.3.9 Conclusions

The purpose of this experiment is to fabricate and characterize lignin-based carbon foams with DDGS additives. The combination of these materials is successfully performed through the pyrolysis of green bodies. The resulting composites form two regimes; a closed packed DDGS matrix, and an open lignin network. These regimes are defined to be Type I, including DDGS-L 25%-75% and DDGS-L 50%-50%; and Type II, including DDGS-L 75%-25% and DDGS-L 90%-10%, respectively. As observed in the results from Ch 2, lignin acts as a pore forming agent for Type I composites and a sintering aid for Type II composites. Both behaviors characterized in the two regimes can be attributed to the liquid phase of lignin, observed between 200 °C and 300 °C during TMA measurements. Thus, lignin acts as a strong binder and sintering aid for these novel carbon foams. Based on the results from Chapters 2 and 3, we can conclude lignin-based foams can be further engineered by adding metals like Cu and waste agricultural feedstock like DDGS.

FUNDING ACKNOWLEDGEMENT

Chapter 2 is funded is by ME Department and Dean Professorship. The third chapter is funded by ND Corn Council.

APPENDICES

APPENDIX A
Tables

Table A1.1: Cu-L Compression; Trial Counts

Trial Counts				
Temp (°C)	300	500	700	900
Cu-L 10-90	5	3	5	5
Cu-L 25-75	5	3	5	5
Cu-L 50-50	5	4	5	5
Cu-L 75-25	5	4	4	5
Cu-100	0	3	3	3

WORKS CITED

[1] N. Alwadani and P. Fatehi, "Synthetic and lignin-based surfactants: Challenges and opportunities," *Carbon Resources Conversion,* vol. 1, no. 2, pp. 126-138, August 2018.

[2] A. Duval and M. Lawoko, "A review on lignin-based polymeric, micro- and nano-structured materials," *Reactive and Functional Polymers,* vol. 85, pp. 78-96, December 2014.

[3] J. Dai, A. F. Patti and K. Saito, "Recent developments in chemical degradation of lignin: catalytic oxidation and ionic liquids," *Tetrahedron Letters,* vol. 57, no. 45, pp. 4945-4951, 9 November 2016.

[4] N. Mahmood, Z. Yuan, J. Schmidt and C. Xu, "Depolymerization of lignins and their applications for the preparation of polyols and rigid polyurethane foams: A review," *Renewable and Sustainable Energy Reviews,* vol. 60, pp. 317-329, July 216.

[5] S. Gupta, M. Dey, C. Matzke, G. Ellis, S. Javaid, K. Hall, Y. Ji and S. Payne, "Synthesis and cahracterization of novel foams by pyrolysis of lignin," *TAPPI JOURNAL,* vol. 18, no. 1, pp. 45-56, January 2019.

[6] Y. Meng, J. Lu, Y. Cheng, Q. Li and H. Wang, "Lignin-based hydrogels: A review of preparation, properties, and application," *International Journal of Biological Macromolecules,* vol. 135, pp. 1006-1019, 15 August 2019.

[7] L. Ming-Fei, S. Shao-Ni, X. Feng and S. Run-Cang, "Sequential solvent fractionation of heterogeneous bamboo organosolv lignin for value-added application," *Separation and Purification Technology,* vol. 101, pp. 18-25, September 2012.

[8] S. Gupta, M. Dey, S. Javaid, Y. Ji and S. Payne, "On the Design of Novel Biofoams Using Lignin, Wheat Straw, and 2 Sugar Beet Pulp as Precursor Material," *ACS Omega,* vol. 5, no. 28, pp. 17078-17089, 2020.

[9] L. Kock-Yee, "Definitions for Hydrophilicity, Hydrophobicity, Superhydrophobicity: Getting the Basics Right," *J. Phys. Chem. Lett.,* vol. 4, no. 5, pp. 686-688, 2014.

[10] M. Sharma, M. P. O. and P. Kumar, "Sysnthesis and Characterization of Copper Foams Through a Powder Metallurgy Route Using a Compressible and Lubricant Space-Holder Material," *International Journal of Minerals, Metallurgy and Materials,* vol. 25, no. 8, p. 902, August 2018.

[11] Y. Y. Zhao, T. Fung, L. P. Zhang and F. L. Zhang, "Lost Carbonate Sintering Process for Manufacturing Metal Foams," *Scripta Materialia,* vol. 52, no. 4, pp. 295-298, February 2005.

[12] R. V. Babu and S. Kanagaraj, "Sintering Behavior of Copper/Carbon Nanotube Composites and Their Characterization," *Adcanced Powder Technology,* no. 30, pp. 2200-2210, 2019.

[13] H. C. de Groh III and B. U. Balachandran, "Conductivity of Copper-Carbon Covetic Composite," *NASA/TM,* 2018.

[14] V. Cheesbrough, K. A. Rosentrater and J. Visser, "Properties of Distillers Grains Composites: A Preliminary Investigation," *J Plym Environ,* no. 16, pp. 40-50, 2008.

[15] J. D. Liaw, D. S. Bajwa, J. Shojaeiarani and S. G. Bajwa, "Corn Disiller's Dried Grains with Solubles (DDGS) - A Value Added Functional Material for Wood Composites," *Industrial Crops and Products,* vol. 139, 1 November 2019.

[16] S. D. Ranathunga, K. F. Kalsheur, J. L. Anderson and K. J. Herrick, "Production of Dairy Cows Fed Distillers Dried Grains with Solubles in Low- and high- forage Diets," *Dairy Sci,* no. 101, pp. 10886-10898.

[17] C. Rimera, M. R. Snowdona, S. Vivekanandhana, X. You, M. Misra, S. Gregori, D. F. Mielewskie and A. K. Mohanty, "Synthesis and Chracterization of Novel Nitrogen Doped Biocarbons from Distillers Dried Grains with Solubles (DDGS) For Supercapacitor Applications," *Bioresource Technology Reports,* vol. 9, February 2020.

[18] N. Zarrinbakhsh, A. K. Mohanty and M. Misra, "Formulation Optimization of Bioreinforced Composites Grom Polyolefins and Dried Distillers' Grains Using Statistical Methods," *Composites Part A: Applied Science and Manufacturing,* no. 119, pp. 246-260, 2019.

[19] B. H. Tisserat, F. J. Eller and M. E. Mankowski, "Properties of Composite Wood Panels Fabricated From Eastern Redcedar Employing Various Bio-Based Green Adhesives," *Bio Resources,* no. 14, pp. 6666-6685, 2019.

[20] B. Tisserat, N. Montesdeoca and V. M. Boddu, "Accelerated Thermal Aging of Bio-Based Composite Wood Panels," *Fibers,* vol. 8, no. 5, 2020.

[21] A. Eksilioglu, N. Gencay, M. F. Yardim and et al., "Mesophase AR Pitch Derived Carbon Foam: Effect of Temperature, Pressure and Pressure Release Time," *J Mater Sci,* no. 41, pp. 2743-2748, 2006.